(DOI will not work until issue is live.) DOI: http://dx.doi.org/10.2138/am.2014.4564

Revision 3

Pluton Assembly and the Genesis of Granitic Magmas: Insights from the GIC Pluton in Cross Section, Sierra Nevada Batholith, California

Keith D. Putirka, Joe Canchola, Jeffrey Rash, Oscar Smith, Gerardo Torrez,
Department of Earth and Environmental Sciences, California State University, Fresno, California 93740, USA

Scott R. Paterson
Department of Earth Sciences, University of Southern California, Los Angeles, California 90089-0740, USA, paterson@usc.edu

Mihai Ducea
Department of Geosciences, The University of Arizona, 1040 E. 4th Street, Tucson, AZ 85721, ducea@email.arizona.edu

ABSTRACT

The ~151 Ma Guadalupe Igneous Complex (GIC) is a tilted, bi-modal intrusion that provides a rare view into the deeper, mantle-derived portions of a granitic pluton. Major oxide relationships show that GIC granitic rocks formed by *in situ* differentiation. Assimilation of sedimentary country rock is precluded, as GIC alumina saturation indices (ASI) are too low by comparison, while TiO_2 and P_2O_5 contents disallow partial melting of metavolcanic lower/middle crust. In contrast, Rb-Sr systematics support *in situ* magmatic differentiation, as unaltered GIC whole rock samples fall on a single 151 Ma isochron (initial $^{87}Sr/^{86}Sr = 0.7036$) matching zircon age dates (Saleeby et al., 1989).

Crystal/liquid segregation, though, was not continuous: mafic and felsic samples form discordant compositional trends, with a gap between 60-66% SiO_2. We posit that crystal/liquid segregation is continuous between 50-60% SiO_2, and leads to intermediate composition liquids that are then too viscous to allow further continuous liquid

segregation. Further crystal/liquid separation thereafter occurs discontinuously (at F ≈ 45-50%), to yield a mafic crystalline (52-59% SiO_2) residue and a silicic (70-75% SiO_2) liquid (Bachmann and Bergantz, 2004), which are respectively preserved in the Meladiorite and Granite/Granophyre units of the GIC. Outcrops in the gabbroic section support this view, where mafic crystalline layers feed directly into granitic dikes, and intermediate compositions are absent; mass balance calculations at the outcrop scale also support this model. It is unclear, though, to what extent this model applies to larger Sierran plutons; the smaller GIC may represent an end-member process, where rapid cooling limits mixing, due to rapid increases in mafic/felsic melt viscosity contrasts.

INTRODUCTION

The Sierra Nevada Batholith (SNB) provides type examples of pluton emplacement (Blanquat et al., 2011; Paterson et al., 2011), and continental crust formation at arcs (e.g., Rudnick, 1995: Tatsumi, 2005; Brown, 2010). Recent work allows for unprecedented detail regarding emplacement of large plutons and batholithic complexes (e.g., Zak et al., 2009; Memeti et al., 2010, and references therein). These studies, however, reveal only the latest stages of upper-level granite emplacement; the underlying processes by which granitic magmas are generated and delivered to a growing magma chamber are mostly hidden from view.

Wiebe and Collins (1998), Robinson and Miller (1999) and Wiebe et al. (2002) demonstrate that granitic magmas are intimately connected to a mafic magma-driven thermal engine, and isotopic studies indicate a role for both mantle- and crust-derived components in Sierran granites (e.g., Kistler and Peterman, 1973; DePaolo and Farmer, 1984; Ague and Brimhall, 1988; Ducea and Saleeby, 1998; Lackey et al., 2008; Cecil et al., 2012, Lackey et al., 2012). What remains unclear is to what extent mantle-derived melts merely provide thermal energy for crustal partial melting, or contribute mass to a growing granitic magma chamber. Studies of mantle xenoliths provide some insights into the gabbro-granite connection (Ducea and Saleeby 1998; Ducea 2002; Lee et al. 2006) but a direct parent-daughter relationship is highly uncertain. And while Noyes et al. (1983) and Ratajeski et al. (2001, 2005) suggest that mafic enclaves are the solid residues of lower crust partial melting, Barbarin (1990) and Dodge and Kistler (1990) show that some enclaves have a magmatic history. Such uncertainties emphasize the need to understand larger mafic systems.

Heterogeneous intrusive bodies of the western Sierra (e.g., Saleeby et al. 1989; Clemens-Knott et al., 2000) allow us to draw a clearer connection between mafic and silicic magmatism (e.g., Dufek and Bergantz 2005; Debari and Greene 2011). An excellent example is the Late Jurassic Guadalupe Igneous Complex (Best, 1963; Figs. 1, 2), or GIC. The GIC is a well-exposed, 151 Ma (Saleeby et al., 1989; Ernst et al., 2009) pluton in the foothills of the Sierra Nevada, north of Fresno California. It contains rocks that range from high MgO gabbros (9 wt. %) to high SiO_2 granites (77 wt. %). The GIC is part of a Jurassic high flux event centered at 161 Ma—a middle phase of development of the Sierra Nevada Batholith (Fig. 2B) and is intruded into arc-related sediments, metavolcanics, and older ophiolitic rocks, partly related to an earlier phase of SNB evolution (Fig. 1; Saleeby 1982; Saleeby, 2011). Unlike larger larger Sierran plutons, it is also strongly bi-modal (Best, 1963). While it is unclear to what extent the GIC provides a model for larger plutons, it likely represents an end-member among a range of processes related to granite formation and pluton assembly.

EARLY WORK & GEOLOGIC BACKGROUND

Host rocks and Tectonic Context

Extensive studies of the western foothills of the Sierra Nevada (e.g., Ransome 1900; Taliaferro, 1942; Best 1963; Clark, 1964; Schweickert, 1978; Saleeby et al. 1978; Saleeby 1982, Schweickert et al. 1984; Bogen 1985; Sharp 1988; Saleeby et al. 1989; Paterson et al. 1991; Clemens-Knott and Saleeby 1999; Herzig and Sharp 1992; Clemens-Knot et al. 2000; Snow 2007; Ernst et al. 2009; Saleeby 2011) show that the region provides key exposures of the pre-batholith crust into which the western parts of the nascent Sierran arc developed, as well as the mafic precursor magmas from which high-elevation granodiorites (e.g., Bateman 1992) are derived. Below is a brief summary of the geologic history of the western Sierran foothills at ~37.5^{o}N.

Phase 1: During the Early to Middle Paleozoic a polygenetic ophiolite formed near a transform fault within the Panthalassa Ocean (Saleeby 2011), well outboard of continental North America (Saleeby et al. 1978). The ophiolite complex was transported along oceanic transform faults and accreted to North America in the Permian, at ~255 Ma (well illustrated in Saleeby 2011, Fig. 16 therein). These ophiolites and accretionary wedge materials formed off the western margin of North America, and served as the host units of Late Triassic to Jurassic arc materials.

Phase 2: Intruding into and overlying the ophiolite-Calaveras mélange is a thick sequence of Late Triassic to Early Jurassic (>192 Ma) volcanics and intrusive rocks

(Saleeby 1982; Herzig and Sharp 1992), which formed part of a Cordilleran-scale arc (Snow 2007) that extended from the Klamath terrane (Sharp 1988; Ernst et al. 2008) to the central Mojave Desert (Miller and Glazner 1995). This arc represents the birth of the SNB.

Phase 3: The Late Triassic-Jurassic volcanics are overlain by younger sediments (e.g., the Mariposa Formation; Bogen 1985; Herzig and Sharp 1992) that formed proximal to western North America (Saleeby et al. 1978). Crosscutting relationships indicate that volcanics and sediments were fully accreted to North America by the Middle Jurassic (Sharp, 1988; Herzig and Sharp 1992; Saleeby 1992; DeCelles 2004). Age dates constrain sedimentation of the Mariposa to 160-153 Ma (Ernst et al. 2009). Simultaneous with Mariposa deposition, plutons of the early SNB, such as the GIC, intruded the growing sedimentary wedge.

The total crustal thickness at 151 Ma is difficult to reconstruct. Regional mapping (Clark 1964; Saleeby 1982; and Schweickert et al. 1984; Paterson et al. 1991) indicates a Late Jurassic crustal thickness of >15 km (Haeussler and Paterson 1993), with the Mariposa Formation representing the upper crust, and metabasalts of the Western Metamorphic Belt and underlying serpentinites, representing the middle to lower crust and upper mantle (Saleeby et al., 1982, 1990). Map patterns in the GIC indicate a vertical plutonic section of 7-8 km. Upper and lower contacts of the GIC are both with the Mariposa Formation; age dates of the Mariposa indicate that its deposition was syn-intrusive (Ernst et al., 2009). Depth to the Moho might approach 20-30 km as Sharp (1988) obtains 6-8 kb pressures for the Chinese Camp ophiolite to the north.

The GIC

Detailed studies of the GIC begin with petrographic and field studies of Best (1963) and Best and Mercy (1967), followed by age dates by Saleeby et al (1989; 151 Ma) and structural studies, which show that the GIC is rotated 28^o along the listric (up-to-the-west) Bear Mountain Thrust Fault (Paterson et al., 1987; Haeussler and Paterson 1993). Mylonites and 151 Ma leucosomes at the base of the GIC (Saleeby et al. 1989) indicate that GIC emplacement was syntectonic. East of the mylonites, however, studies show that the GIC is largely undeformed and represents a structurally intact pluton (Tobisch et al. 1987; Vernon et al. 1989; Paterson et al. 1991; Haeussler and Paterson 1993). Ernst et al. (2009) recently obtained an age of 153±2 Ma from multiple single zircon SHRIMP measurements, which overlap bulk zircon TIMS dates (150-151 Ma; Saleeby et al. 1989).

Our work is the first petrologic study of GIC since Best (1963), who compared the GIC to classic layered mafic intrusions (e.g. Wager 1960; Wager et al. 1960). While the gabbros of the GIC are indeed layered, most layers are fine-grained basaltic “intramagmatic flows” (Wiebe et al. 2002) that probably intrude along rheological contrasts (Wiebe et al. 2002). At higher structural levels these flows are emplaced into granitic magma (e.g., Frost and Mahood 1987; Wiebe et al. 2002). Best (1963) used the term “agmatite” (Sederholm, 1923) to describe that part of the GIC between the gabbros and structurally higher granitoids, which he thought formed by mafic roof collapse into a granite magma chamber. However, his agmatite unit displays considerable evidence for mafic-felsic magma mingling, so we abandon the term in favor of “Mingled Zone”.

METHODS

Our high density sampling allowed us to examine a near complete cross section of a Sierran pluton, and test for bimodality and paleodepth-dependent composition trends. We analyzed 560 samples for major oxides (Table A1, Electronic Appendix), about 1/6th of which are examined in thin section. The GIC samples are from CA State Route 140 and Old Highway, which offer near-vertical cross sections of the GIC, the Hornitos Road, which provides a profile through middle portions of the complex (Fig. 2), and Indian Gulch Road, which provides limited outcrops of the lowest parts of the exposed section. We also sample the Mariposa Formation both east and west of the GIC along Route 140 (Fig. 2), the Western Metamorphic Belt metavolcanics, which outcrop throughout the map area (Fig. 1), gabbros from the nearby (and as yet unmapped) Hornitos pluton, and rhyolites that overlie the GIC. The Hornitos may represent a feeder zone to the GIC (Putirka et al. 2014), but further study is needed to verify this hypothesis.

In our revised map (Fig. 2), the various units of the GIC have the following areal proportions: Gabbro (upper and lower) + Meladiorite, 46% (the Gabbro/Meladiorite boundary is uncertain); Mingled Zone, 32%; Granite and Granophyre, 22%. The gabbro section is likely much larger as the base of the GIC is not exposed (Hauessler and Paterson, 1993).

Major elements are analyzed by wavelength dispersive X-ray fluorescence spectrometry, at the California State University, Fresno, using sample powders that are calcined so as to dehydrate each sample and oxidize Fe to Fe^{3+}. Sample preparation and analytical details are provided in Busby et al. (2008). Relative errors for USGS standards are as follows: BCR-2: SiO_2: 0.55%; TiO_2: 0.89%; Al_2O_3: 0.67%; Fe_2O_3: 0.36%; MgO: 0.28%; CaO: 0.28%; Na_2O: 0.01%; K_2O: 0.56%; P_2O_5: 0.01%. GSP-2: SiO_2: 0.15%;

TiO_2: 1.5%; Al_2O_3: 0.01%; Fe_2O_3: 0.20%; MgO: 4.1%; CaO: 0.94%; Na_2O: 2.13%; K_2O: 0.37%; P_2O_5: 0.01%.

Whole rock isotopic ratios (Table 2) of $^{87}Sr/^{86}Sr$ and Rb and Sr concentrations are determined by thermal ionization mass spectrometry. Rock powders are dissolved in mixtures of hot concentrated HF-HNO_3 in large Savillex vials, spiked with the Caltech (unmixed) Rb and Sr spikes. Rb, Sr were separated on cation columns containing AG50W-X4 resin, using 1N to 4N HCl. Rb is loaded onto single Re filaments using silica gel and H_3PO_4. Strontium is loaded onto single Ta filaments with Ta_2O_5 powder.

Mass spectrometric analyses are carried out at the University of Arizona on an automated VG Sector multicollector instrument fitted with adjustable 10^{11} Faraday collectors and a Daly photomultiplier (Otamendi et al. 2009). Concentrations of Rb and Sr are determined by isotope dilution, with isotopic compositions determined on the same spiked runs. Typical runs consist of 100 isotopic ratios. Ten runs of the standard NRbAAA performed during the course of this study yield a mean $^{85}Rb/^{87}Rb$ or 2.61199±20. Fifteen analyses of NIST standard NBS987 yielded a mean $^{87}Sr/^{86}Sr$ of 0.710265±7 and $^{84}Sr/^{86}Sr$ of 0.056316±12. The Sr isotopic ratios of standards and samples are normalized to $^{86}Sr/^{88}Sr = 0.1194$. The estimated analytical ±2σ uncertainties are: $^{87}Rb/^{86}Sr = 0.25\%$ and $^{87}Sr/^{86}Sr = 0.0012\%$. Procedural blanks averaged from five determinations are 10 and 150 pg for Rb and Sr respectively.

RESULTS

Best (1963) and Best and Mercy (1967) provide detailed petrographic descriptions of each intrusive unit, and our new work, except where noted, confirms their observations;

we thus provide only general petrographic descriptions, or observations that are new. Our references to the "upper" or "top" of the pluton refer to features that point towards the felsic rocks to the east, while "lower" or "bottom"-directed features point towards the Gabbro unit to the west (Fig. 2). Unit names are capitalized; rock names are not.

While the GIC provides a remarkable opportunity to study a Sierran pluton in cross section, outcrops are on private property, and can only be accessed along public roads. In the descriptions that follow, we provide lithologic relationships for a few rare exposures, nearly all of which were observed and described by Best (1963). A key advance is our high-density sampling, which provides reveals top-to-bottom compositonal patterns of the pluton, and enables rigorous testing of mass balance and fractionation processes. Like Best (1963), we find that the GIC is bi-modal—much more so than larger Sierran plutons, such as the Tuolumne Intrusive Complex (TIC) (Memeti et al. 2014, and NAVDAT http://www.navdat.org/) and Bass Lake Tonalite (BLT; NAVDAT).

GIC Gabbro

Best (1963) divided the base of the GIC into "lower" and "upper" Gabbro, but we do not distinguish these in our new map (Fig. 2). Gabbros from both the upper and lower parts of the unit are fine- (<1mm) to medium-grained (1-5 mm) equigranular, and contain clinopyroxene (cpx) + plagioclase (pl) ± hornblende (hbl) ± olivine (ol) ± orthopyroxene (opx). The upper and lower Gabbro units have a similar wide-ranging mineralogy (e.g., 10-40% cpx) but upper Gabbro samples have less olivine (0-10%, compared to as much as 20% at the very base of the lower Gabbro), and more hornblende (up to 50% in some layers, compared to <10% in the lower Gabbro); but we see no field or petrographic bases on which to draw a boundary. The Gabbro samples are mostly hypidiomorphic-intergranular, and as noted by Best (1963) ophitic textures are rare. Plagioclase is optically unzoned and hornblendes lack reaction rims and appear to be in equilibrium with other minerals. Rare stream-washed areas in the upper Gabbro expose chilled margins and load-cast features, the latter of which have sense-of-tops pointed upwards, towards the felsic part of the pluton. Outcrop and thin section characteristics are strikingly similar to sheeted sill complexes at Onion Valley (Sisson et al. 1996) and Goodale Canyon (Coleman et al. 1995), and intramagmatic flows described by Wiebe and Collins (1998) and Wiebe et al. (2002).

Stream-washed exposures of the upper Gabbro reveal alternating centimeter- to meter-scale bands of black fine-grained layers and reddish medium-grained layers (Figs. 5A, C), with sharp boundaries. Most of our Gabbro samples are not from stream-washed areas, and so layering is generally not visible. But our stream-washed-derived samples show that the black, finer-grained layers consist mostly of pl and hbl, with lesser amounts of cpx and opx, and exhibit no internal differentiation; these layers tend towards an ophitic texture, and plagioclase laths are often elongated, and oriented parallel to the direction of layering. In contrast, reddish layers consist of pl and cpx (Fig. 5C) and intersertal textures are more common; three samples from one 4 cm-thick reddish layer show decreasing MgO towards the top (samples G1A-7A, -6B, -6A, Table A1, range from 7.08, 6.86 and 5.84% MgO respectively). Reddish layers also all have distinctly higher SiO_2 (>53%, except for one sample with 51%) compared to black layers (<53%).

Mafic samples from the GIC Gabbro unit (and the nearby Hornitos pluton) have MgO and SiO_2 contents that range from 4.5—9.0% and 49.4—54.5 wt. % respectively (Fig.

(DOI will not work until issue is live.) DOI: http://dx.doi.org/10.2138/am.2014.4564

6A), and at least three suites can be distinguished. The fine-grained upper Gabbro samples have the highest TiO_2, Fe_2O_3 and K_2O at a given MgO, and show no internal variations of TiO_2 (Fig. 6B) and Fe_2O_3 (Fig. 6C), despite exhibiting slight but noticeable variations with respect to K_2O and SiO_2 (Figs. 6A, D). Samples of the lower Gabbro in Fig. 6 are olivine-rich samples and are similar to rocks describe by Best (1963); these have lower TiO_2, Fe_2O_3 and K_2O compared to upper Gabbro black layers. The reddish layers in the upper Gabbro samples are yet lower still in TiO_2 and Fe_2O_3 at a given MgO. Hornitos exposures are poor, and make it more challenging to differentiate distinct units there, but those samples fall on the high K_2O, TiO_2 and Fe_2O_3 ends of the lower Gabbro and fine-grained upper Gabbro trends.

Felsic Dikes Within Upper Gabbro Stream-washed areas of the upper Gabbro show that the black, fine-grained gabbroic layers are cut by tension gashes filled by coarse-grained (5-30 mm) felsic materials. The felsic dikes consist of pl + quartz + potassium feldspar + hbl + biotite ± zircon ± olivine (fayalite-rich). The tension gashes are <1.4 m in length; <25 cm at their greatest width (Fig. 5D), often surrounded by vesiculated gabbro haloes. Where present, they comprise <5% of local outcrop area. Some felsic dikes are open in the downwards direction, and have hbl + pl crystalline residues at their base, which appear to be fed by the coarser, reddish gabbroic layers (Fig. 5E). The dikes are oriented perpendicular to the strike of the gabbroic layers, but some occur at slight angles to the gabbroic layers, as if infilling Andersonian cracks.

Meladiorite

Meladiorite is a term used by Best (1963) to describe rocks with abundant hornblende (so the rocks are melanocratic). But the Meladiorite map unit is lithologically quite diverse (although not well exposed). Many Meladiorite rocks are identical to each of the rock types of the upper Gabbro unit. Most rocks are fine- to medium-grained, equigranular, and consist of pl + hbl ± cpx ± biotite ± sphene ± apatite, with rare quartz and olivine. Plagioclase grains often have overgrowth rims (see Best, 1963). Compared to the Gabbro unit hbl (>20%) is in excess of pyroxene (often absent, but up to 20% in the Meladiorite). The Meladiorite samples also contain biotite, titanite and apatite, all of which are absent from gabbros. The majority of the Meladiorite rocks are medium-grained and have up to 80% of either hbl or pl, and so likely repesent crystalline residues; but the Meladiorite also contains fine-grained rocks with "mafic-intermediate" compositions (54.9-59.4% SiO_2) that lack phenocrysts and quite likely represent liquids. Like the gabbros below, the Meladiorite also contains felsic segregations (72.7-75.2 % SiO_2), which are medium- rather than coarse-grained, and occur not as dikes but as small pods (0.5 m) or large oblong masses (10-20 m) oriented parallel to the layering of the GIC. Lithologic relationships with adjacent rocks are not often clearly exposed, but one small outcrop yields sharp contacts with coarsely crystalline biotite and hbl-rich rocks.

We locate the Meladiorite based on the first appearance of biotite moving up in the section, which places the base of the Meladiorite unit much deeper than noted by Best (1963), but it's base is can only be observed along road cuts, so its map extent is dashed (Fig. 2). Best (1963) also mapped the felsic segregations of the Meladiorite as quartz monzonite, but most have sufficient quartz to be classified as granite and are so shown in Figure 2. Mineral abundances do not change systematically from top to bottom within the

(DOI will not work until issue is live.) DOI: http://dx.doi.org/10.2138/am.2014.4564

Meladiorite unit, but when felsic segregations are excluded, mean whole rock SiO_2 contents increase slightly from ~53 to ~56 wt. % from bottom to top. The Meladiorite also ranges to higher SiO_2 (49-62.6% SiO_2) compared to the upper Gabbro (49.4-52.9 wt. % SiO_2).

The Mingled Zone (Best's "Agmatite")

Overlying the Meladiorite is what we term the "Mingled Zone" (Fig. 2) (Best's "agmatite"), where fine- to medium-graned mafic and mafic-intermediate rocks (compositionally and petrographically identical to Meladiorite and Gabbro samples) intrude into a host identical to the Granite unit. Figure 8A shows the top of the Mingled Zone exposed along highway 140, west of Mariposa, CA. This exposure shows a series of sub-parallel basaltic layers intruding into a granitic host. The largest, middle sheet has sharp contacts that bound a massive gabbro, while most other layers are accumulations of pillow-like mafic enclaves (Fig. 8A). Boundaries between enclaves and host are sharp, but enclaves only rarely have chilled margins. Figure 8B shows a rounded mafic enclave surrounded by a rim of granitic host with part of the host intruding into the enclave. Outcrop characteristics are suggestive of the intramagmatic flows of Wiebe and Collins (1998) and Wiebe et al. (2002). These intrusions also clearly show the dike-disaggregation features modeled by Snyder and Tait (1995).

Except for having slightly higher K_2O (0.5-0.9 wt. % K_2O) than the gabbros (0.1-0.2 wt. % K_2O; Fig. 7), mafic samples from the Mingled Zone are otherwise identical to Gabbro samples (Table 1). Granitic host materials of the Mingled Zone are also compositonally similar to the Granites above. Like the Gabbro and Granite units that are below and above, respectively, Mingled Zone felsic and mafic rocks form distinctly discordant major oxide trends that intersect at ~63% SiO_2; this discordance is most dramatic with respect to SiO_2 vs. Na_2O and SiO_2 vs. Al_2O_3 (Fig. 7). Enclave compositions are mostly independent of size; however, a few small enclaves (<10 cm) have MgO<6%, while the remainder have MgO≥6%. All but one of five transects across mafic enclaves (>10 cm in dia; Table A1) and into adjacent host material show that enclave cores and rims are compositionally identical, and that host materials both adjacent and far from enclave contacts have identical compositions

GIC Granitic units

Above the Mingled Zone are the overlying Granite and Granophyre (Fig. 2) units. The Granophyre is defined by an abrupt upward transition into rocks where granophyre-textured intergrowths are more common, and where such texturees begin to comprise a larger fraction (up to 60%) of any given sample. Both the Granite and Granophyre units are texturally mixed, however: some Granite samples contain as much as 10% granophyre, especially near the top of the unit, while some Granophyre samples lack such textures entirely. Coarse-grained granitic rocks are more common compared to Gabbro samples, but most rocks from both the Granite and Granophyre are fine- to medium-grained equigranular, with grain sizes mostly <1.5 mm. The rocks consist of varying amounts of quartz + pl + hbl + Fe-Ti oxides + biotite ± sphene ± apatite. Rounded and zoned plagioclase feldspar phenocrysts 2 to 4 mm long comprise less 5% of most rocks. Many feldspars have fritted cores containing sericite ± cholrite, and rims that preserve albite twinning—textures indicative of alteration (e.g., albitization, Plümper and Putnis

(DOI will not work until issue is live.) DOI: http://dx.doi.org/10.2138/am.2014.4564

2009). Average SiO_2 for the non-enclave granitic host increases only slightly from the bottom of the Granite (71.8% SiO_2) to top of the Granophyre unit (73.3 wt. %). Rocks with 69-77 wt. % SiO_2 can be found at any paleodepth. Both the Granite and Granophyre units contain mafic enclaves (SiO_2<60 wt. %), the abundances of which decrease dramatically upwards from the top of the Mingled Zone. Mafic enclaves are compositionally identical to those found in the Mingled Zone and range in MgO to as high as 9 wt. % in the Granite unit, and 5.5 wt. % at the top of the Granophyre.

Except for Na_2O, Granite and Granophyre samples are similar to one another, and to Mingled Zone host rocks, as well as felsic dikes and pods found in lower units (Fig. 9). Mean and maximum SiO_2 contents increase slightly upwards (minimum/maximum SiO_2 values are: Mingled Zone, 71.0/76.5; Granite, 73.1/77.6; Granophyre, 74.2, 79.1) (Fig. 9), but these units are not strongly zoned. We do find, however, that at the top of the pluton, the Na_2O contents of a subset of Granite and Granophyre samples are high enough to be readily separated using the following equation:

$$\text{Na-index} = Na_2O - 22.5 + 0.246[SiO_2] \qquad \text{at } SiO_2>66.1 \text{ wt. \%} \qquad \text{Eqn. (1)}$$

This line (Fig. 9A) separates lower Na_2O Grante and Granophyre samples that are similar to Mingled Zone host rocks (negative Na-index) from a subset of Granite and Granophyre samples with distinctly higher Na_2O (positive Na-index) at a SiO_2 content. Equation (1) applies only to rocks with >66% SiO_2.

DISCUSSION

Below, we examine how the different parts of the GIC were generated, and devise a model for pluton assembly.

Albitization of some Granite and Granophyre Samples

Before interpreting magmatic events it is essential to exclude samples that show evidence of post-magmatic alteration. At the GIC, some Granite and Granophyre samples appear to be albitized. Some rocks have a positive Na-index (Eqn. 1; Fig. 9A), and for these, Na-indices are inversely correlated with K_2O (Fig. 10A), indicating Na-K exchange. In thin section, these same samples show textural evidence of albitization (hydrothermal replacement of orthoclase by albite; Kaur et al., 2012; Plümper and Putnis, 2009). Na-index values also increase towards the top of the pluton (Fig. 10B), indicating top-down alteration. Given that Mariposa Formation sediments have very low Na_2O/K_2O ratios relative to the GIC, assimilaiton of the Mariposa itself cannot be responsible for albitization. Since the Mariposa sediments, into which the GIC was intruded, are hemipelagic (Clark, 1964; Herzig and Sharp, 1992), though, ambient seawater is a likely high Na_2O/K_2O metasomatizing agent.

Age and Depth of Emplacement of the GIC

New isotope data show that all unaltered GIC samples fall upon a single Rb-Sr isochron (Fig. 11), that yields an age of 151 ± 7 Ma (with a MORB-like initial $^{87}Sr/^{86}Sr$ of 0.7036), which is identical to the zircon-based date of Saleeby et al. (1989), and within error of the 153 ± 2 Ma date of Ernst et al. (2009). Not included in the isochron regression line are granitic samples with high Na-indices, which fall to very low Rb/Sr ratios; we posit that Rb, as well as K were lost at some later time. One low-K_2O granitic sample (G 13.5), however, falls close to the isochron, and if this sample is added to the regression, the age increases to 153±6 Ma.

As to emplacement depth, our observations support Haussler and Paterson's (1993) model that the GIC was emplaced at depths that are shallower than typical for SNB plutons. For example, granophyric intergrowths, which are common in the uppermost parts of the GIC, have long been ascribed to rapid cooling during epizonal pluton emplacement (e.g., Buddington 1959). A large undercooling (70-150 ^{o}C), rather than pressure, is the key variable for their development (Morgan and London 2012), but the requisite high undercoolings can be obtained under such conditions (2-4 km, e.g., Lowenstern et al. 1997). As already noted, albitization of the GIC also points to a shallow emplacement.

Mineral-liquid equilibria also point to low-*P* magmatic equilibration for the GIC, compared to the Tuolumne Intrusive Complex and the Bass Lake Tonalite. The normative quartz-albite-orthoclase (Q-Ab-Or) pseudo-ternary (Fig. 12) has long been used as a means to estimate equilibration pressures for granitic systems (e.g., Tuttle and Bowen 1958; Luth et al. 1964; Ebadi and Johannes 1991; Holtz et al. 1992; Blundy and Cashman 2001). These studies show that high-SiO_2 liquids with quartz and alkali feldspar require equilibration at low pressures. Figure 12 provides a highly imperfect barometer as some compositions may represent mechanical mixtures rather than equilibrated phases—but many granitic GIC samples are fine-grained and likely approximate liquids (Fig. 9). Lower magmatic equilibration pressures are thus plausible for the GIC, given its higher mean Q content (Fig. 12). This does not imply, however, that low-Q samples that approach the 1000 MPa cotectic are high *P* liquids. Trends towards lower Q are plausible low-*P* crystallization paths (Tuttle and Bowen 1958; Holtz et al. 1992; Blundy and Cashman 2001), and some GIC samples that fall between the 200-1000 MPa curves have no quartz, so the cotectics would not apply. In any case, granophyre and albitization textures and Q-Ab-Or ternary relationships indicate shallower emplacement depths for the GIC compared to the Bass Lake Tonalite and Tuolumne Intrusive Complex.

Mafic and Mafic-intermediate Magmas (50-59% wt. SiO_2)

Throughout the GIC we find highly mafic (>8-9% MgO) fine-grained rocks (Table 1, A1), either as layers within the Gabbro or Meladiorite, or as enclaves within the Mingled Zone or Granite units. These rocks are probably too evolved to represent direct partial melts of the mantle; they have Mg# (molar MgO/[FeO + MgO]) ratios of 0.65-0.67, while mantle-derived melts should have Mg#s > 0.69 (Kinzler 1997; Gaetani and Grove 1998). But given their repeatability within the section, and their high Mg#s, they are probably only minimally fractionated and may represent a density minimum along a fractionation path (curve F0; Fig. 6B) involving more mafic compositions stalled at Moho depths (Stolper and Walker, 1980; Glazner and Ussler, 1988). For these and subsequent models of fractional crystallization, we follow Hanson and Langmuir (1978) and Langmuir and Hanson (1981) in modeling major oxides, by applying the Rayleigh distillation model: $C_i^{liq} = C_i^o F^{[Di\text{-}1]}$, where C_i^{liq} = concentraiton of i in a fractionated liquid, C_i^o = concentration of i in original unfractionated liquid, F = melt fraction, D_i = bulk distribution coefficient of i. Details of our approach and sample calculations are provided in Appendix B; best fit values for D_i are given in the relevent figure captions.

Mafic-intermediates (50-61% SiO_2) are dominant in the Meladiorite and Mingled Zone units, but also occur as thin reddish medium-grained crystalline-residue layers in the upper Gabbro. Major oxide trends (Fig. 7) show that their compositional ranges cannot represent mixing with felsic end-member magmas (SiO_2 of ~75%). So samples at the high end of the SiO_2 range, i.e., 59-61% SiO_2 must either differentiate directly from less evolved mafic-intermediates, form by mixing with a composition that is near the compositional gap (~63% SiO_2), or form outside the GIC mafic system (i.e., by crustal partial melting, and so by accident produce a trend that is suggestive of *in situ* fractionation or mixing). The mafic-intermediates are also comprised of not one, but multiple compositional trends, most evident with respect to SiO_2-TiO_2 (Fig. 7E), but also in SiO_2-Al_2O_3 and SiO_2-P_2O_5 (Figs. 7D, H). These compositional trends can be explained by fractionating varying proportions of plagioclase and hornblende from observed mafic rocks with 7-9% MgO (Figs. 7, 14; Table 1). This hypothesis is supported by the presence of plausible crystalline residues in the Meladiorite, with plagioclase- and hornblende-rich rocks containing up to 80% of either mineral (and grain sizes of 1-2 mm), as well as very fine-grained samples (mean grain size <0.5 mm) with SiO_2 = 50-59% SiO_2, which are –plausible intermediate liquids. Most likely, such rocks form by a range of fractionation processes, with mingling and mixing between various fractionated products.

Origin of granitic (75% SiO_2) magmas

Several processes for generating granitic magmas have been proposed, including direct fractionation of basaltic parent magmas (e.g., Bowen 1928, and more recently Jagoutz 2010), partial melting of upper crust felsic materials (e.g., sediments, Chappell 1999), partial melting of hydrous, mafic lower crust (e.g., Noyes et al. 1983; Beard and Lofgren, 1991; Ratajeski et al. 2001) and separation of immiscible liquids (Roedder

1951; Philpotts 1976; VanTongeren and Mathez, 2012). Our field and geochemical observations allow us to evaluate these models.

Partial Melts of the Crust or Liquid Immiscibility?

We reject partial melting of upper crust for several reasons. The upper crust is composed of the Mariposa Formation, and as already noted, it has Na_2O/K_2O ratios that are too low to allow bulk assimilation to form GIC granitic rocks. Also, as might be expected (Chappell et al. 2012), the Mariposa has high alumina saturation indices (ASI) (avg. = 2.8±1.7; Fig. 13A). But in the GIC, all but a few mylonitized samples within the Bear Mountains Fault zone fall to a much lower ASI at a given SiO_2 (Fig. 13A). Only one sample from the Mariposa Formation approaches the GIC field in ASI – SiO_2 space (EXCR-5), and it is the one sample furthest removed from the pluton. And the few mylonitized samples that trend towards high ASI might not represent upper crust partial melts, but rather mechanical mixtures of Mariposa sediments and felsic melts that penetrated the then-active Bear Mountains Fault zone.

Lower crust partial melting can also be rejected for the vast majority of GIC samples. Metavolcanics in the map area (Fig. 1) have lower TiO_2 and higher P_2O_5 at a given level of differentiation compared to GIC samples, which we show as P_2O_5/TiO_2 vs. SiO_2 (Fig. 13B). Ratios of P_2O_5/TiO_2 are much higher for metavolcanics on the whole compared to the GIC samples at any given SiO_2. Both P^{5+} and Ti^{4+} are high field strength elements and are thus unlikely to be mobilized by fluid alteration or metamorphism, and no apatite is observed in the metavolcanic rocks. It is thus unlikely that partial melting of these rocks can produce the GIC granites with low P_2O_5/TiO_2 ratios, let alone reproduce the very coherent P_2O_5/TiO_2 vs. SiO_2 trends for mafic and felsic GIC samples (Fig. 13B).

Interestingly, a few Meladiorites have elevated P_2O_5/TiO_2 (>0.25), and are allowably derived as large degree partial melts of the metavolcanic materials. A subset of GIC Granites (and mylonitized felsic samples at the base of the GIC) also has high P_2O_5/TiO_2 at a given SiO_2. These samples can be separated using a P/Ti-index:

P/Ti-index = $P_2O_5/TiO_2 – (0.009[SiO_2] +0.87)$ at $SiO_2 > 66.9$ wt. % Eqn. 2a

P/Ti-index = $P_2O_5/TiO_2 – (0.007[SiO_2] +0.2)$ at $SiO_2 < 66.9$ wt. % Eqn. 2b

where all oxides are in weight %, and where a high P/Ti-index may indicate partial melting of a metavolcanic source. Some GIC granites have a positive P/Ti-index and are allowably derived as partial melts of the metavolcanics; but these represent just a small fraction of all GIC felsic samples (12% of the 178 non-mylonitized GIC samples with >65% SiO_2), based on our high-density sampling of the Granite, Granophyre and upper Mingled Zone units.

As to liquid immiscibility, Charlier and Grove (2013) suggest that calc-alkaline, hydrous magmas, like the GIC, are unlikely to intersect the two–liquid solvus (at the GIC, even rocks with 8-9% MgO contain magmatic hornblende). But their work provides a surer compositional test. Figure 13C shows that Fe, P, K and Ti are in combination too low to allow immiscibility for GIC liquids at any SiO_2 content (Fig. 13C).

Magmatic Fractionation: Promises and Problems

Several lines of evidence support direct magmatic fractionation as the origin of GIC granitic compositions. First, Rb-Sr isotopic ratios allow that all GIC rock types are generated by closed system crystallization differentiation. Unaltered samples, ranging from high MgO gabbros to granitic rocks with 75% SiO_2, fall on a single Rb-Sr isochron (Fig. 11), which yields an age of 151±7 Ma, identical to that obtained by single crystal zircon studies (150-153 Ma; Saleeby et al. 1989; Ernst et al. 2009). This result does not rule out metabasalt partial melting, since in combination a few select metabasalt samples may yield the correct initial $^{87}Sr/^{86}Sr$ (Table 2); but as noted, P/Ti indices suggest that partial melting of metavolcanics is limited.

However, if *in situ* magmatic fractionation was operative, major oxide trends indicate multiple fractionation paths. Of the three gabbroic suites (lower Gabbro, and the reddish and black layers of the upper Gabbro), none can be derived from the others by fractional crystallization, although each trend (FC1 and FC2; Fig. 6B) can be generated by fractionation of a more mafic parent (with ~12-15% MgO; Fig. 6B) that precipitates only olivine (FC0). Curves FC1 and FC2 can then be produced by liquids that later become multiply saturated. It is not clear whether these fractionation trends are generated *in situ*, or at greater depths and then delivered to a shallower GIC chamber. Regardless, fractional crystallization of observed gabbro phases reproduces felsic dike compositions (FC3). High-density sampling in stream-washed exposures, though, reveals no intermediate compositions (Fig. 6), and at the map scale, intermediate compositions (60-66% SiO_2) are rare, and so crystal mush/liquid extraction appears to be discontinuous.

<u>The Role of Intermediate Compositions (60-66% SiO_2) and Magma Mixing</u>

A key result of our major oxide analyses is that felsic (>66% SiO_2) and mafic (<60% SiO_2) samples fall on distinctly discordant major-oxide trends (Figs. 7, 14) that mutually approach the gap in SiO_2 at ~63 wt. %. This discordance is notable in the Harker diagrams, especially with respect to SiO_2 vs. Na_2O (Fig. 14A): Na_2O increases with increasing SiO_2 for mafic samples, but decreases with increasing SiO_2 for felsic samples. Such compositional trends clearly cannot be generated by mixing of end-member mafic and felsic magmas. But they can be produced if either (a) a Na changes from incompatible to compatible, as fractionated liquids approach 63% SiO_2, or (b) felsic end-member liquids (~75% SiO_2) mix with intermediate magmas having ~63% SiO_2. Option (a) could be accomplished by precipitation of plagioclase, and the formation of a plagioclase-rich crystalline residue. And indeed, the trend of granitic rocks in Fig. 7D point directly towards two fine-grained, plagioclase-rich samples from the Meladiorite (MDJC-3C, -3E). However, these same samples are not viable as crystalline residues as they have Na_2O and P_2O, and total Fe as Fe_2O_3 (Fe_2O_3t) that are too low to explain felsic compositonal trajectories. Indeed, most rocks that appear to be crystalline residues (medium-grained, with high proportions of either amphibole or plagioclase) fall within the cluster of samples with 54-59% SiO_2 and so cannot explain the granitic compositional trends. Fractional crystallization models involving an intermediate parent liquid yield curved evolutionary paths that fail to match such trends precisely (e.g., Fig. 9B). The highly linear trends amongst the felsic samples (66-77% SiO_2; Figs. 7, 9) are better described by magma mixing. In any case, both mafic and felsic suites converge at 63% SiO_2, which seems to indicate that intermediate liquids, despite their paucity, may have played a key role in GIC evolution. A problem, of course, is that such magmas are rare. Of 243 samples analyzed from the Meladiorite and Mingled Zone, only 20 samples (8.2%) have SiO_2 contents between 60 and 68 wt. %, and only 8 samples fall within the 60-64% SiO_2 range. If intermediate liquids were dominant, subsequent differentiation processes must have been highly efficient.

Evidence for *In Situ* Processes

The upper Gabbro unit provides compelling field evidence that fractionation, at least locally, occurred *in situ*. Felsic dikes there are far too small to allow for significant magma-filled crack propagation, and have clear field relationships linking their origin to a residue consisting of the medium-grained reddish layers with 53-54% SiO_2 (Fig. 5E). Smaller felsic pods within the Meladiorite also appear to be generated *in situ*, and may have formed within solidification fronts as described by Marsh (2002). This leaves open the possibility that the same process(es) that generated felsic dikes and Meladiorite pods also generated the massive granites at the top of the pluton. Felsic dikes of the Gabbro unit and the felsic pods of the Meladiorite overlap compositions from the Granite, Granophyre and Mingled Zone at the top of the GIC (Fig. 9). Meter-scale reddish layers within the Gabbro and Meladiorite units also point to the evolution of much larger felsic dikes, as do granitic pods throughout the Meladiorite—large enough to segregate from crystalline residues.

Compositional trends for the GIC indicate an *in situ* origin for GIC granite. If the bi-modal GIC represents the infilling of a shallow chamber by two genetically unrelated felsic and mafic melts, these two melts (Granite and Gabbro) would almost certainly have experienced some mixing with one another. But no such mixing is evident (despite evidence for extensive mingling). Instead, the trajectory for rocks with 75% SiO_2 (Figs. 7, 9, 14) is towards a composition with ~60-63% SiO_2 (and ~3 wt. % MgO and ~4.5 wt. % Na_2O; Fig. 9). The discordant mafic (<63% SiO_2) and felsic (>63% SiO_2) major oxide trends (e.g., Fig. 14) are more readily developed if intermediate and felsic rocks both form by *in situ* processes (by generation and mixing with an intermediate liquid composition layer). If *in situ* processes are not dominant, then some mechanism is needed to allow recharge mafic magmas to intrude the granite, but that only allows their fractionated products to actually mix with the resident felsic magmas. We grant that most mafic and mafic-intermediate GIC samples are fine- to medium-grained, indicating that they are chilled upon intruding a cooler, pre-existing granitic magma body. However, granitic dikes in the gabbro are clearly *in situ* and nonetheless emanate from fine- to medium-grained compacted layers. GIC bi-modality is also not explained if magmas are generated at depth and then delivered to emplacement depths, as any crustal density structure that allows upward delivery of mafic and felsic magmas should also deliver intermediate compositions.

Discontinuous Crystal Much/Liquid Separation Processes

Models proposed by Brophy (1991) and Bachmann and Bergantz (2004) yield a promising means to explain compositional bi-modality. In the Bachmann and Bergantz (2004) model, an intermediate bulk composition crystallizes to form a residual and highly viscous felsic liquid, at which point settling of crystals is greatly hindered (see also Brophy, 1991); interstitial felsic liquids aggregate through compaction, and when melt fractions (F) reach 0.5-0.7 (Bachmann and Bergantz 2004; Dufek and Bachmann 2010), the felsic liquid can buoyantly segregate. In this way, an intermediate bulk composition is differentiated into a bi-modal mass of mafic crystals and felsic liquid, leaving a compositional gap between the two. Mass balance supports this model at both the outcrop and pluton scale. At the outcrop scale, the felsic segregations (73.2% SiO_2) of the upper Gabbro can be generated from an intermediate magma by subtracting the reddish crystalline residues (53.9% SiO_2). The predicted F is 0.45 to 0.60 if the intermediate magma (prior to crystal-liquid separation) has 62.6 to 65% SiO_2 (Table 1). These F

values are consistent with the proportions of felsic and crystalline residual materials within the upper Gabbro (when they are found intact, Fig. 5D), and in the range of theoretical estimates of *F* that allow for mineral-felsic liquid separation (Dufek and Bachmann 2010). At the pluton scale we use an average of all Meladiorite samples with SiO_2<60% as a model crystalline residue and an average of all high SiO_2 compositions (75.6% SiO_2) as a residual liquid; if an intermediate parent has 63% SiO_2, the resulting melt fractions (F = 0.45-0.55) approach the theoretical critical values. This model explains bi-modality in that it is those liquids that have 60-66% SiO_2 that are (apparently efficiently) differentiated to form much of the Meladiorite and Gabbro (as crystalline residues) and the Granite and Granophyre as evolved liquids. The areal fraction of GIC granitic rocks supports this argument. For example, the putative intermediate magma (63% SiO_2) can be generated by fractional crystallization of parental gabbroic magmas (8% MgO) at $F \approx 0.35$ (Figs. 14). The total amount of expected granite end-member (75.6% SiO_2) is thus 35% multiplied by the 45%-55% felsic liquid obtained in the mass balance, or ≈16-19% total. Granitic outcrops comprise ~22% of the outcrop area and contain 73% SiO_2 on average. Mixing calculations show that this mean composition can be obtained as a 79%-21% mix of end-member (75.6% SiO_2) and intermediate (63% SiO_2) magmas. So the observed amount of felsic end-member magma in the Granite + Granophyre units is 79% x 22% = 17.4% of the GIC by area, and so within the expected 16-19% range just cited. To this must be added the amount of end-member granite in the Mingled Zone, which is highly uncertain, but we suppose that it is 3% of the total GIC area—this raises the total granite end-member to ≈21%. This is only slightly above the 16-19% predicted by our major oxide fractionation modeling, but given that the base of the complex is not exposed, this 21% estimate is almost certainly a maximum value. This maximum value is consistent with phase equilibria experiments of Sisson et al. (2005), where granitic melts (75% SiO_2) are produced at total F = 12-25%. The Sisson et al. (2005) experimental granite liquids also accurately reproduce the compositions of felsic GIC samples, and their experimental crystalline residues match Meladiorite mineralogies. Although Sisson et al. (2005) argued for a lower crust partial melting model to generate Sierran granites, their experiments (which do not distinguish between up- and down-temperature processes), as well as observed GIC major oxides, mineralogy, isotopes, and experimental data, are consistent with an *in situ* origin for GIC granitic rocks.

Some Caveats

A few fine-grained compositions from the Granite and Meladiorite units indicate the presence of plausible intermediate composition liquids (Fig. 14). However, these samples are few, and the Bachmann-Bergantz model does not predict felsic (>66% SiO_2) major-oxide trends (Figs. 14). To apply the Bachmann-Bergantz model, it must be assumed that the melt expulsion process is highly efficient, leaving few un-fractionated intermediates. This indeed appears to be the case for the felsic dikes within the Gabbro unit, which may serve as an outcrop-scale model for the GIC as a whole. An obvious alternative is that felsic GIC rocks were produced by a continuous crystal/liquid segregation process, but it is not clear how such a process would create a bi-modal pluton, and such a model would not produce linear major oxide trends for GIC samples with >66% SiO_2. One might still argue that rocks in the range 60-66% SiO_2 were generated, but consumed by later mixing and homogenization. But to lose intermediate compositions by mixing necessarily implies the simultaneous loss of highly evolved magmas—and rocks with 74-77% SiO_2

are abundant in the GIC. We thus tentatively conclude that mineral-liquid separation in the Bachmann-Bergantz process was efficient.

IMPLICATIONS

Assembly of a Pluton

Our high-density sampling of the GIC delimits both the genesis of felsic magmas and the assembly of the GIC pluton, for which we offer a preliminary model (Figure 15):

Stage 1: Hydrous, basaltic magmas, parental to the GIC, form by differentiation at the base of the crust; achieving sufficient buoyancy (e.g., increases in H_2O; Ochs and Lange 1999), these magmas serially intrude as sills into a shallow chamber (Bachmann et al. 2011) that occupies Triassic arc crust.

Stage 2: Magmas from Stage 1 differentiate to yield intermediate (50-63% SiO_2) magmas by continuous crystal/liquid separation. Intermediates with ~63% SiO_2 differentiate into felsic magmas (~75% SiO_2) and mafic crystalline residues (50-55% SiO_2) through a discontinuous crystal/liquid separation process (Bachmann-Bergantz, 2004; their Fig. 2). The felsic magma chamber grows incrementally as highly felsic liquids (75% SiO_2) are expelled upwards into a growing felsic cap. This is similar to Bachl et al. (2001) or Harper et al. (2004), except GIC recharge magmas are mafic, and all intermediate and felsic liquids form *in situ*.

Stage 3: At a critical thickness, the felsic magma cap convects to allow mixing with intermediate melts below; convection distributes mixtures of such throughout the felsic reservoir (as at Aztec Wash; Robinson and Miller 1999).

Stage 4: Final cooling occurs as mafic inputs diminish, and the supply of thermal energy to the felsic chamber subsides. The uppermost parts of the GIC, being furthest removed from this waning heat source, experience the greatest undercoolings, yielding granophyric intergrowths.

The general implications of this 4-stage model for pluton genesis, and tectonics, are yet to be fully developed. It is not clear, for example, whether all GIC granitic materials were generated *in situ*, or whether lower crust partial melting generated some fraction. We are also unsure to what extent the GIC serves as a model for Sierran granites. The GIC has many compositional similarities with more massive intrusions (Bateman 1992), but these larger plutons are not similarly bi-modal (Fig. 3). Being <1/10th the size of the Tuolumne Intrusive Complex, the GIC certainly had a much shorter thermal lifespan (Blanquat et al. 2011; Paterson et al., 2011; Melekhova et al. 2013); with rapid cooling, mafic/felsic melt viscosity contrasts may have increased too quickly to allow magma mixing (Sparks and Marshall 1986; Frost and Mahood, 1987). Whatever the cause of such contrasts, our 4-stage model may describe an end-member amongst a range of genetic possibilities. Finally, at the tectonic scale, the GIC's MORB-like initial $^{87}Sr/^{86}Sr$ ratios (see also Clemens-Knott et al. 2000) show that asthenospheric material clearly contributed to the arc system near the height of Late Jurassic melt production—when a mafic crystalline root was supposedly being developed, rather than degraded (DeCelles et al. 2009); the asthenosphere thus appears to play a role at all stages of batholith genesis.

ACKNOWLEDGEMENTS

The authors thank all the participants and co-leaders of the 2012 Penrose Field Forum, "Formation of the Sierra Nevada Batholith: Magmatic and Tectonic Processes and Their Tempos". We thank Bob Wiebe, Cin-Ty Lee and Chip Lesher for very fruitful on-the-outcrop discussions. These discussions were of great help and substantially influenced the present work. We also thank Bob Wiebe and Calvin Miller for extremely helpful and detailed formal reviews, and Associate Editor Chip Lesher for his review and comments. Keith Putirka thanks the students enrolled in Igneous and Metamorphic Petrology at Fresno State in the years 2006 and 2012, and Megan McNaughton, Joshua Marroquin, Keith Thompson, and Wynter Erickson who contributed greatly to the initial reconnaissance phases of field and geochemical studies of the GIC. We also thank Vali Memeti for use of her TIC compositions, Jade Star Lackey for very fruitful discussions about Sierra magmatism and isotope geochemistry. We thank Barbara Ratschbacher and Nate Nicodemus for their help in drafting Figure 1. We also thank Matt Paige for sharing previous results (not used in this paper) of GIC chemistry studies and Myron Best for sending a digital version of his original map of the GIC. This work is supported by NSF grant: EAR-1250322.

Ague, J.J., and Brimhall, G.H. (1988) Magmatic arc asymmetry and distribution of anomalous plutonic belts in the batholiths of California: effects of assimilation, crustal thickness, and depth of crystallization. Geological Society of America Bulletin, 100, 912-927.

Arculus, R.J. (2003) Use and abuse of the terms calcalkaline and calcalkalic. Journal of Petrology, 44, 929-935.

Bachl, C.A., Miller, C.F., Miller, J.S., and Faulds, J.E. (2001) Construction of a pluton: evidence form an exposed cross section of the Searchlight pluton, Eldorado Mountains, Nevada. Geological Society of America Bulletin, 113, 1213-1228.

Bachmann, O., and Bergantz, G.W. (2004) On the origin of crystal-poor rhyolites: extracted from batholithic crystal mushes. Journal of Petrology, 45, 1565-1582.

Bachmann, O., Deering, C.D., Ruprecht, J.S., Huber, C., Skopelitis, A., and Schnyder, C. (2011) Evolution of silicic magmas in the Kos-Nisyros volcanic center, Greece: a petrological cycle associated with caldera collapse. Contributions to Mineralogy and Petrology, doi:10.1007/s00410-011-0663-y.

Barbarin, B. (1990) Plagioclase xenocrysts and mafic magmatic enclaves in some granitoids of the Sierra Nevada Batholith, California. Journal of Geophysical Research, 95, 17747-17756.

Bateman, P.C. (1992) Plutonism in the central part of the Sierra Nevada Batholith, California. U.S. Geol Surv. Prof. Paper 1483, 186 p.

Beard, J.S., and Lofgren, G.E. (1991) Dehydration melting and water-saturated melting of basaltic and andesitic greenstones and amphibolites at 1, 3, and 6.9 kbar. Journal of Petrology, 32, 365-401.

Best, M.G. (1963) Petrology of the Guadalupe Igneous Complex southwestern Sierra Nevada foothills, California. Journal of Petrology, 4, 223-259.

Best, M.G., and Mercy, E.L.P. (1967) Composition and crystallization of mafic mineral in the Guadalupe Igneous Complex, California. American Mineralogist, 52, 436-474.

Blanquat, M., Horsman, E., Habert, G., Morgan, S., Vanderhaeghe, O., Law, R., and Tikoff, B. (2011) Multiscale magmatic cyclicity, duration of pluton construction, and the paradoxical relationship between tectonism and plutonism in continental arcs. Tectonophysics, 500, 20-33.

Blundy, J. and Cashman, K. (2001) Ascent-driven crystallization of dacite magmas at Mount St. Helens, 1980-198. Contributions to Mineralogy and Petrology, 140, 631-650.

Bogen, N.L. (1985) Stratigraphic and sedimentologic evidence of a submarine island-arc volcano in the lower Mesozoic Peñon Blanco and Jasper Point Formations, Mariposa Co., California. Geological Society of America Bulletin, 96, 1322–1331.

Bowen, N.L. (1928) The evolution of the igneous rocks. Dover Publications, NY, 332 p.

Brophy, J.G. (1991) Composition gaps, critical crystallinity, and fractional crystallization in orogenic (calk-alkaline) magmatic systems. Contributions to Mineralogy and Petrology, 109, 173-182.

Brown, M. (2010) The spatial and temporal patterning of the deep crust and implications for the process of melt extraction. Philosophical Transactions of the Royal Society A, 368, 11-51.

Buddington, A.F. (1959) Granite emplacement with special reference to North America. Geological Society of American Bulletin, 70, 671-747.

Busby, C.J., Hagan, J., Putirka, K., Pluhar, C., Gans, P., Rood, D., DeOeo, S., Skilling, I. Wagner, D. (2008) The ancestral Cascades arc: Implications for the development of the Sierran microplate and tectonic significance of high K_2O volcanism, in, J. Wright and J. Shervais (eds.) Ophiolites, Arcs and Batholiths, Geological Society of America Special Paper 438, 331-378.

Cecil, M.R., Rotberg, G.L., Ducea, M.N., Saleeby, J.B., and Gehrels, G.E. (2012) Magmatic growth and batholithic root development in the northern Sierra Nevada, California. Geosphere, 8, 592-606, doi:10.1130/GES00729.1.

Chappell, B.W. (1999) Alumina saturation in I- and S-type granites and the characterization of fractionated haplogranites. Lithos, 49, 535-551.

Chappell, B.W., Bryant, C.J., and Wyborn, D. (2012) Peraluminous I-type granites. Lithos, 153, 142-153.

Charlier, B., and Grove, T.L. (2012) Experiments on liquid immiscibility along tholeiitic liquid lines of descent. Contributions to Mineralogy and Petrology, 164, 27-44.

Clark, L.D. (1964) Stratigraphy and structure of part of the western Sierra Nevada metamorphic belt, California. U.S. Geological Survey Professional Paper, P 0410, 70 p.

Clemens-Knott, D., and Saleeby, J.B. (1999) Impinging ring dike complexes in the Sierra Nevada batholith, California: Roots of the Early Cretaceous volcanic arc. Geological Society of America Bulletin, 111, 484-496.

Clemens-Knott, D., Wolf, M.B., and Saleeby, J.B. (2000) Middle Mesozoic plutonism and deformation in the western Sierra Nevada foothills, California, in Lageson, D.R., Peters, S.G., and Lahren, M.M., eds., Great Basin and Sierra Nevada, Geological Society of America Field Guide 2, p. 205-221.

Coleman, D.S., Bartley, J.M., Glazner, A.F., and Pardue, M.J. (2012) Is chemical zonation in plutonic rocks driven by changes in source magma composition or shallow-crustal differentiation? Geosphere, 8, doi:10.1130/GES00798.1.

Coleman, D.S., Glazner, A.F., Miller, J.S., Bradford, K.J., Frost, T.P., Joye, J.L., and Bachl, C.A. (1995) Exposure of a Late Cretaceous layered mafic-felsic magma system in the central Sierra Nevada batholith, California. Contributions to Mineralogy and Petrology, 120, 129-136.

DeBari, S.M., and Greene, A.R. (2011) Vertical stratification of composition, density and inferred magmatic processes in exposed arc crustal sections, in Brown, D., and Ryan, P.D., eds., Arc-Continent Collision, Frontiers in Earth Sciences, p. 121-144, Springer Verlag, Berlin.

DeCelles, P.G., Ducea, M.N., Kapp, P., and Zandt, G. (2009) Cyclicity in Cordilleran orogenic systems. Nature Geoscience, doi:/10.1038/NGEO469.

DeCelles, P.G. (2004) Late Jurassic to Eocene evolution of the Cordilleran thrust belt and foreland basin system, western U.S.A. American Journal of Science, 304, 105-168.

DePaolo, D.J. and Farmer, G.L. (1984) Isotopic data bearing on the origin of Mesozoic and Tertiary granitic rocks in the western United States. Philosophical Transactions of the Royal Society of London, A310, 743-753.

Dodge, F.C.W., and Kistler, R.W. (1990) Some additional observations on inclusions in the granitic rocks of the Sierra Nevada. Journal of Geophysical Research, 95, 17841-17848.

Ducea, M.N. (2002) Constraints on the bulk composition and root foundering rates of continental arcs: A California perspective. Journal of Geophysical Research, 107, doi:/10.1029/2001JB000643

Ducea, M.N., and Saleeby, J.B. (1998) The age and origin of a thick mafic-ultramafic keep from beneath the Sierra Nevada batholith. Contributions to Mineralogy and Petrology, 133, 169-185.

Dufek, J. and Bachmann, O. (2010) Quantum magmatism: magmatic compositional gaps generated by melt-crystal dynamics. Geology, 38, 687-690.

Dufek, J., and Bergantz, G.W. (2005) Lower crustal magma genesis and preservation: a stochastic framework for the evaluation of basalt-crust interaction. Journal of Petrology, 46, 2167-2195.

Ebadi, a., and Johannes, W. (1991) Beginning of melting and composition of first melts in the system Qz-Ab-Or-H_2O-CO_2. Contributions to Mineralogy and Petrology, 106, 286-295.

Ernst, W.G., Snow, C.A., and Scherer, H.H. (2008) Contrasting early and late Mesozoic petrotectonic evolution of northern California. Geological Society of America Bulletin, 120, 179-194

Ernst, W.G., Saleeby, J.B., and Snow, C.A. (2009) Guadalupe pluton – Mariposa formation age relationships in the southern Sierra Foothills: onset of Mesozoic subduction in northern California. Journal of Geophysical Research, 114, doi:10.1029/2009JB006607.

Frost, B.R., Barnes, C.G., Collins, W.J., Arculus, R.J., Ellis, D.J., and Frost, C.D. (2001) A geochemical classification for granitic rocks. Journal of Petrology, 42, 2033-2048.

Frost, T.P. and Mahood, G.A. (1987) Field, chemical and physical constraints on mafic-felsic magma interaction in the Lamarck Granodiorite, Sierra Nevada, California. Geological Society of America Bulletin, 99, 272-291.

Gaetani, A.G., and Grove, T.L. (1998) The influence of water on melting of mantle peridotite. Contributions to Mineralogy and Petrology, 131, 3232-346.

Gill, J.B. (1981) Orogenic andesites and Plate Tectonics, Berlin Germany, Springer, 390 p.

Glazner, A.F., and Ussler, III, W. (1988) Trapping of magma at midcrustal density discontinuities. Geophysical Research Letters, 15, 673-675.

Haeussler, P.J., and Paterson, S.R. (1993) Timing, burial and uplift of the Guadalupe Igneous Complex, Sierra Nevada, California. Geological Society of America Bulletin, 105, 1310-1320.

Hanson, G.H., and Langmuir, C.H. (1978) Modelling of major elements in mantle-melt systems using trace element approaches. Geochmica et Cosmochimica Acta, v. 42, p. 725-741.

Harper, B.E., Miller, C.F., Koteas, C., Cates, N.L., Wiebe, R.A., Lazzareschi, D.S., and Cribb, J.W. (2004) Granites, dynamic magma chamber processes and pluton construction: the Aztec Wash pluton, Eldorado Mountains, Nevada, USA. Transactions of the Royal Society of Edinburgh: Earth Sciences, 95, 277-295.

Herzig, C.T., and Sharp, W.D. (1992) The Sullivan Creek terrane: A composite Jurassic arc assemblage, western Sierra Nevada metamorphic belt, California. Geological Society of America Bulletin, 104, 1292-1300.

Holtz, F., Pichavant, M., Barbey, P., and Johannes, W. (1992) Effects of H_2O on the liquidus phase relations in the haplogranite system at 2 and 5 kbar. American Mineralogist, 77, 1223-1241.

Jagoutz, O.E. (2010) Construction of the granitoid crust of an island arc. Part II: a quantitative petrogenetic model. Contributions to Mineralogy and Petrology, 160, 359-381.

Kaur, P., Chaudhri, N., Hofmann, A.W., Raczek, I., Okrusch, M., Skora, S., and Baumgartner, L.P. (2012) Two-stage extreme albitization of A-type granites from Rajasthan, NW India. Journal of Petrology, 53, 919-948.

Kinzler, R.J. (1992) Melting of mantle peridotite at pressures approaching the spinel to garnet transition: application to mid-ocean ridge basalt peterogenesis. Journal of Geophysical Research, 102, 853-874.

Kislter, R.W., and Peterman, Z.E. (1973) Variations in Sr, Rb, K, Na and initial Sr^{87}/Sr^{86} in Mesozoic granitic rocks and intruded wall rocks in central California. Geological Society of America Bulletin, 84, 3489-3512.

Kuno, H. (1968) Differentiation of basalt magmas, in Hess, H.H., and Poldervaart, A.A. (eds.) Basalts: The Poldervaart Treatise on Rocks of Basaltic Composition, 2, New York, NY, Interscience, 623-688.

Lackey, J.S., Valley, J.W., Chen, J.H., and Stockly, D.F. (2008) Dynamic magma systems, crustal recycling, and alteration in the central Sierra Nevada Batholith: the oxygen isotope record. Journal of Petrology, 49, 1397-1426.

Lackey, J.S., Cecil, M.R., Windham, C.J., Frazer, R.E., Bindeman, I.N., and Gehrels, G.E. (2012) The Fine Gold Intrusive Suite: the roles of basement terranes and magma source development n the Early Cretaceous Sierra Nevada batholith. Geosphere, 8, doi: 10.1130GES00745.1.

Langmuir, C.H., and Hanson, G.H. (1981) Calculating mineral-melt equilibria with stoichiometry, mass balance, and single component distributions coefficients. In Newton, R.C., Navrotsky, A., and Wood, B.J., Eds., Thermodynamics of Minerals and Melts: Advances in Physical Geochemistry Volume 1, p. 247-271, Springer-Verlag, New York.

Le Bas , M.J., Le Maitre, R.W., Streckeisen, A., and Zanettin, B. (1986) A chemical classification of volcanic rocks based on the total alkali-silica diagram. Journal of Petrology, 27, 745-750.

Lee, C-T., Cheg, X., and Horodyskyj, U. (2006) The development and refinement of continental arcs by primary basaltic magmatism, garnet pyroxenite accumulation, basaltic recharge and delamination: insights from the Sierra Nevada California. Contributions to Mineralogy and Petrology, 151, 222-242.

Lowenstern, J.B., Clynne, M.A., and Bullen, T.D. (1997) Comagmatic A-Type granophyre and rhyolite from the Alid volcanic center, Eritrea, northeast Africa. Journal of Petrology, 38, 1707-1721.

Luth, W.C., Jahns, R.H., and Tuttle, O.F. (1964) The granite system at pressures of 4 to 10 kilobars. Journal of Geophysical Research, 69, 759-773.

Marsh, B.D. (2002) On bimodal differentiation by solidification front instability in basaltic magmas, part 1: Basic mechanics. Geochmica et Cosmochimica Acta, 66, 2211-2229.

Memeti, V., Paterson, S., Matzel, J., Mundil, R., and Okaya, D. (2010) Magmatic lobes as “snapshots” of magma chamber growth and evolution in large, composite batholiths: an example from the Tuolumne intrusion, Sierra Nevada California. Geological Society of America Bulletin, 122, 1912-1931.

Memeti, V., Paterson, S., and Mundil, R. (2014) Day 4: Magmatic evolution of the Tuolumne Intrusive Complex. In, Memeti, V., Paterson, S.R., and Putirka, K.D., eds., Formation of the Sierra Nevada Batholith: Magmatic and Tectonic Processes and Their Tempos, Geological Society of America Field Guide 34, Geological Society of America, in press.

Melekhova, E., Annen, C., and Blundy, J. (2013) Compositional gaps in igneous rock suites controlled by magma system heat and water content. Nature Geoscience, doi:10.1038/NGEO1781, 385-390.

Miller, J.S., and Glazner, A.F. (1995) Jurassic plutonism and crustal evolution in the central Mojave Desert, California. Contributions to Mineralogy and Petrology, 118, 379-395.

Miyashiro, A. (1974) Volcanic rock series in island arcs and active continental margins. American Journal of Science, 274, 321-355.

Morgan, G.B. and London, D. (2012) Process of granophyre crystallization in the Long Mountain Granite, southern Oklahoma. Geological Society of America Bulletin, doi: 10.1130/B30569.1.

Noyes, H.J., Wones, D.R., and Frey, F.A. (1983) A tale of two plutons: petrographic and mineralogic constraints on the petrogenesis of the Red Lake and Eagle Peak plutons, central Sierra Nevada, California. Journal of Geology, 91, 353-379

Ochs, F.A., III, and Lange, R.A. (1999) The density of hydrous magmatic liquids. Science, 283, 1314–1317.

Otamendi, J.E., Ducea, M.N., Tibaldi, A.M., Bergantz, G.W., de la Rosa, J.D., and Vujovich, G.I. (2009) Generation of Tonalitic and Dioritic Magmas by Coupled Partial

Melting of Gabbroic and Metasedimentary Rocks within the Deep Crust of the Famatinian Magmatic Arc, Argentina. Journal of Petrology, 50, 841-873.

Paige, M., Brophy, J., and Dorais, M. (1996) Evaluation of differentiation mechanisms in the layered calc-alkaline Guadalupe Igneous Complex, Catheys Valley, CA. Geological Society of America, Abstracts with Program. 28, p. 483.

Paterson, S. (2012) Tectonic Evolution of the Cordilleran Orogeny in the Central Sierra Nevada: Integrating Detrital Zircon Dating With Mapping, Structural, and Plutonic Studies. Geological Society of America Abstracts with Programs, 44, p. 174.

Paterson, S.R., Memeti, V., Mundil, R. (2010) ICP-MS and TIMS zircon dating in the Sierra Nevada: Initial implications for tectonic and magmatic processes: Geological Society of America Abstracts with Programs, v. 42, p. 46.

Paterson, S.R., Okaya, D., Memeti, V., Economos, R., and Miller, R.B. (2011) Magma addition and flux calculations of incrementally constructed magma chambers in continental margin arcs: combined field, geochronologic, and thermal modeling studies. Geosphere, 7, 1439-1468, doi:10.1130/GES00696.1.

Paterson, S.R., Tobisch, O.T., and Radloff, J.K. (1987) Post-Nevadan deformation along the Bear Mountains fault zone: implications for the Foothills Terrane, central Sierra Nevada, California. Geology, 15, 513-516.

Paterson, S.R., Tobisch, O.T., and Vernon, R.H. (1991) Emplacement and deformation of granitoids during volcanic arc construction in the foothills terrane, central Sierra Nevada, California. Tectonophysics, 191, 89-110.

Peacock, M.A. (1931) Classification of igneous rock series. Journal of Geology, 39, 54-67.

Philpotts, A.R. (1976) Silicate liquid immiscibility: its probably extent and petrogenetic significance. American Journal of Science, 276, 1147-1177.

Plümper, O., and Putnis, A. (2009) The complex hydrothermal history of granitic rocks: multiple feldspar replacement reactions under subsolidus conditions. Journal of Petrology, 50, 967-987.

Putirka, K.D., Canchola, J., McNaughton, M., Smith, O., Torrez, G., Paterson, S.R., and Ducea, M. (2014) Day 1: Guadalupe Igneous Complex. In, Memeti, V., Paterson, S.R., and Putirka, K.D., eds., Formation of the Sierra Nevada Batholith: Magmatic and Tectonic Processes and Their Tempos, Geological Society of America Field Guide 34, Geological Society of America, in press.

Ratajeski, K., Glazner, A.F., and Miller, B.V. (2001) Geology and geochemistry of mafic to felsic plutonic rocks in the Cretaceous intrusive suite of Yosemite Valley, California. Geological Society of American Bulletin, 113, 1486-1502.

Ratajeski, K., Sisson, T.W., and Glazner, A.F. (2005) Experimental and geochemical evidence of the El Capitan Granite, California, by partial melting of hydrous gabbroic lower crust. Contributions to Mineralogy and Petrology, 149, 713-734.

Ransome, F.L. (1900) Mother Lode district. U.S. Geological Survey Geological Atlas, Folio 63, 11p.

Robinson, D.M., and Miller, C.F. (1999) Record of magma chamber processes preserved in accessory mineral assemblages, Aztec Wash pluton, Nevada. American Mineralogist, 84, 1346-1353.

Roedder, E. (1951) Low-temperature liquid immiscibility in the system K_2O-FeO-Al_2O_3-SiO_2. American Mineralogist, 36 282-286.

Rudnick, R.L. (1995) Making continental crust. Nature, 378, 571-578.

Saleeby, J.B. (1982) Polygenetic ophiolite belt of the California Sierra Nevada: Geochronological and tectonostratigraphic development. Journal of Geophysical Research, 87, 1803–1824.

Saleeby, J.B. (1992) Petrotecotnic and paleogeographic settings of U.S. Cordilleran ophiolites, in Burchfiel, G.C., Lipkman, P.W., and Zoback, M.L., eds., The Cordilleran orogen: Coterminous U.S., Geological Society of America, The Geology of North America, G-3, 107-168.

Saleeby, J. (2011) Geochemical mapping of the Kings-Kaweah ophiolite belt, California—Evidence for progressive mélange formation in a large offset transform-subduction initiation environment. In Wakabayashi. J., Dilek, Y., eds., Melanges: processes of formation and Societal significant: Geological Society of America Special Paper 480, 31-73.

Saleeby, J.B., Geary, E.E., Paterson, S.R., and Tobisch, O.T. (1989) Isotopic systematics of U-Pb (zircons) and Ar^{40}/Ar^{39} (biotite/hornblende) from rocks of the central foothills terrane, Sierra Nevada, California. Geological Society of America Bulletin, 101, 1481-1492.

Saleeby, J.B., Goodin, S.E., Sharp, W.D., and Busby, C.J. (1978) Early Mesozoic paleotecotonic-paleogeographic reconstruction of the southern Sierra Nevada region. In Howell, D.G., and McDougall, K.A., eds., Mesozoic Paleogeography of the Western United States, Pacific Coast Paleogeography Symposium 2, p. 311-336, Pacific Section of the Society of Economic Paleontologists and Mineralogists, Los Angeles, CA.

Schweickert, R.A. (1978) Triassic and Jurassic paleogeography of the Sierra Nevada and adjacent regions, California, and western Nevada. In Howell, D.G., and McDougall, K.A., eds., Mesozoic Paleogeography of the Western United States, Pacific Coast Paleogeography Symposium 2, p. 361-384, Pacific Section of the Society of Economic Paleontologists and Mineralogists, Los Angeles, CA.

Schweickert, R.A., Bogen, N.L., Girty, G.H., Hanson, R.E., and Merguerian, C. (1984) Timing and structural expression of the Nevadan orogeny, Sierra Nevada, California. Geological Society of America Bulletin, 95, 967–979.

Sederholm, J.J., 1923, On migmatites and associated pre-Cambrian rocks of southwestern Finland. Part I, the Pellinge region. Bulletin de la Commission Géologique de la Finlande, 58, 1–153.

Sharp, W.D. (1988) Pre-Cretaceous crustal evolution in the Sierra Nevada region, California. In Ernst, W.G. (ed.) Metamorphism and crustal evolution of the western United States, Prentice Hall, Englewood Cliffs, N.J., p. 824-864.

Sisson, T.W., Grove, T.L., and Coleman, D.S. (1996) Hornblende gabbro sill complex at Onion Valley, CA, and a mixing origin for the Sierra Nevada Batholith. Contributions to Mineralogy and Petrology, 126, 81-108.

Sisson, T.W., Ratajeski, K., Hankins, W.B., and Glazner, A.F. (2005) Voluminous granitic magmas from common basaltic sources. Contributions to Mineralogy and Petrology, 148, 635-661.

Snow, C.A. (2007) Petrotectonic evolution and melt modeling of the Peñon Blanco arc, central Sierra Nevada foothills, California. Geological Society of America Bulletin, 119, 1014-1024.

(DOI will not work until issue is live.) DOI: http://dx.doi.org/10.2138/am.2014.4564

Snow, C.A., and Ernst, W.G. (2008) Detrital zircon constraints on sediment distribution and provenance of the Mariposa Formation, central Sierra Nevada Foothills, California. In Wright, J.E., ed., Arcs, Ophiolites, and Batholiths: A volume in Honor of Clifford Hopson, Geological Society of America Special Paper 438.

Snyder, D., and Tait, S. (1995) Replenishment of magma chambers: comparison of fluid mechanic experiments with field relations. Contributions to Mineralogy and Petrology, 122, 230-240.

Sparks, R.S.J. and Marshall, L.A. (1986) Thermal and mechanical constraints on mixing between mafic and silicic magmas. Journal of Volcanology and Geothermal Research, 29, 99-124.

Stacey, J.S., and Kramers, J.D. (1975) Approximation of Terrestrial Lead Isotope Evolution by a 2-Stage Model. Earth and Planetary Science Letters 26, 207-221.

Stolper, E., and Walker, D. (1980) Melt density and the average composition of basalt. Contributions to Mineralogy and Petrology, 74, 7-12.

Taliaferro, N.L. (1942) Geologic history and correlation of the Jurassic of southwestern Oregon and California. Geological Society of America Bulletin, 53, 71-112.

Tatsumi, Y. (2005) The subduction factory: how it operates in the evolving Earth. GSA Today, 15, 4-10.

Tobisch, O.T., Paterson, S.R., Longiaru, S., and Bhattacharyya, T. (1987) Extent of the Nevadan orogeny, central Sierra Nevada, California, Geology, 15, 132-135.

Tuttle, O.F., and Bowen, N.L. (1958) Origin of granite in the light of experimental studies in the system $NaAlSi_3O_8$-$KAlSi_3O_8$-SiO_2-H_2O. Geological Society of America Memoir, 74, 153 p.

VanTongeren, J.A., and Mathez, E.A. (2012) Large-scale liquid immiscibility at the top of the Bushveld Complex. Geology, 40, 491-494.

Vernon, R.H., Paterson, S.R., and Geary, E.E. (1989) Evidence for syntectonic intrusion of plutons in the Bear Mountains fault zone, California. Geology, 17, 723-726.

Wiebe, R.A., Blair, K.D., Hawkins, D.P., and Sabine, C.P. (2002) Mafic injections, *in situ* hybridization, and crystal accumulation in the Pyramid Peak granite, California. Geological Society of America Bulletin, 114, 909-920.

Wiebe, R.A., and Collins, W.J. (1998) Depositional features and stratigraphic sections in granitic plutons: implications for the emplacement and crystallization of granitic magmas. Journal of Structural Geology, 20, 1273-1289.

Wager, L.R. (1960) The major element variation of the layered series of the Skaergaard Intrusion and a re-estimation of the average composition of the hidden layered series and of the successive residual magmas. Journal of Petrology, 1, 364-398.

Wager, L.R., Brown, G.M., and Wadsworth, W.J. (1960) Types of igneous cumulates. Journal of Petrology, 1, 73-85.

Zak, J., and Paterson, S. (2009) Magmatic erosion of the solidification front during reintrusion: the eastern margin of the Tuolumne batholith, Sierra Nevada, California. International Journal of Earth Science, doi: 10.1007/s00531-009-0423-7.

Zak, J., Paterson, S., Janousek, V., and Kabele, P. (2009) The Mammoth Peak sheeted complex, Tuolumne batholith, Sierra Nevada California: a record of initial growth or late thermal contraction in a magma chamber. Contributions to Mineralogy and Petrology, 158, 447-470.

This is a preprint, the final version is subject to change, of the American Mineralogist (MSA)
Cite as Authors (Year) Title. American Mineralogist, in press.
(DOI will not work until issue is live.) DOI: http://dx.doi.org/10.2138/am.2014.4564 3/5

FIGURE CAPTIONS

Figure 1. Map of regional geology in the vicinity of the Guadalupe Igneous Complex.

Figure 2. (A) Geologic map of the Guadalupe Igneous Complex, after Best (1963). Our map replaces Best's "agmatite" with Mingled Zone. The lower boundary of the Meladiorite is defined based on the appearance of biotite; "quartz monzonites" within the Meladiorite are now shown as Granite. We also do not distinguish between an "upper" and Lower" Gabbro because while olivine modes increase slightly downwards, there is no distinct field or petrographic characteristic that allows for a straightforward distinction (most "lower" gabbro samples, for example, contain hornblende). (B) Histogram of zircon ages (Paterson et al. 2010; Paterson 2012) showing three main pulses of magmatism in the evolution of the Sierra Nevada Batholith. Individual age dates are from detrital zircons from sediments (Sedimentary) and igneous rocks (Igneous), whose distributions are shown individually using green and gray bars respectively. Statistics for each peak are for the sum of the ages (Sed + Ign), shown as uncolored bars. The GIC, at 151 Ma, is part of the Jurassic pulse of magmatic activity.

Figure 3. Major element igneous rock classification schemes, with a comparison of the Guadalupe Igneous Complex (GIC) to the Tuolumne Igneous Complex (TIC). A: Peacock (1939) diagram; B: Fe# (FeO/(FeO+MgO), wt. % ratio) vs. SiO_2 classification scheme of Frost et al. (2001); C: AFM diagram of Kuno (1968); A = total alkalis, F = FeO, M = MgO as weight fractions; D: Alumina silica index (ASI) classification of

Chappell et al. (2012) where ASI (sometimes known as an "A/CNK ratios") are is the mole fraction ratio: Al_2O_3/[CaO – 1.67(P_2O_5) + Na_2O + K_2O], and SiO_2 is in weight %; E: K_2O vs. SiO_2 with boundaries from Gill (1981); F: total alkalis vs. SiO_2 of Le Bas et al. (1986). TIC and BLT data (Memeti et al., 2013; NAVDAT, http://www.navdat.org) are restricted to samples with 97-102 wt. % totals, renormalized to 100 wt. % to compare to calcined GIC compositions.

Figure 4. Histogram of SiO_2 contents for the Guadalupe Igneous Complex (GIC; green bars) and the Tuolumne Igneous Complex (TIC; dashed black outline). Inset shows mean values and standard deviations for SiO_2 for felsic portions of both suites (SiO_2>62.5 wt. %). The felsic portions of the GIC are clearly much more silicic on average compared to the TIC, as well as other Sierran granitoids.

Figure 5. Photomicrographs of layers in the upper Gabbro, showing a sharp contact between coarser- and finer-grained gabbro bands (A), and the granophyre texture (from the granophyre unit), from the uppermost part of the GIC (B). C shows field context for Gabbro layers in A (lens cap is 6 cm in diameter). The reddish layers in C correspond the hornblende (hbl)-absent coarser-grained layers at the bottom half of A, while dark layers in C correspond to the hbl-bearing finer-grained layers in the upper half of A. Contacts both above and below the reddish coarse-grained layers are mostly sharp, but C shows a gradational lower contact with finer-grained material below. D shows felsic dikes that cut through the upper gabbro layers. (E) shows the base (directed down towards the mafic

part of the pluton) of one dike apparently being fed by a reddish layer, between which is a hbl + pl crystalline residue. A hbl rim about the felsic dike is also evident, probably caused by reaction with gabbro host as water is expelled from the dike upon cooling; some dikes (not shown) have vesiculated haloes (3-4 cm in width).

Figure 6. MgO vs. SiO_2 (A), TiO_2 (B), Fe_2O_3 (C), and K_2O (D) for Gabbro rock types; "lower" Gabbro samples are olivine-rich layers at the very base of the section, which are similar to rocks classified as such by Best (1963), but are not a distinguishable map unit in our study. Inset panel in D shows a magnified view of MgO vs. K_2O; curves labeled FC0-3 are fractional crystallization curves (parameters noted below). These panels compare black (fine-grained) and reddish (medium-grained) layers from stream-washed areas of the upper Gabbro (Fig. 5A, C). We also plot felsic dikes from the upper Gabbro (Figs. 5C-F), and "other samples" from the upper Gabbro, which derive from non-stream washed areas where the layering is likely present, but not visible. We also compare rocks from the lower Gabbro and the mafic portion of the Hornitos. The finer-grained black layers form a small array of increasing SiO_2 with decreasing MgO, which can be explained by fractional crystallization of observed phases, but these rocks show no internal differentiation of TiO_2 and Fe_2O_3. Coarser-grained reddish gabbros, in contrast, show internal differentiation of TiO_2 and Fe_2O_3, and have very different TiO_2, Fe_2O_3 and K_2O at the same MgO, so none (coarse- and fine-grained upper gabbros, and lower gabbros) can be derived by direct fractionation from one another; however, FC0 shows that each suite can be derived by fractional crystallization of a more mafic parent. The Hornitos gabbros appear to contain slightly more differentiated examples of each of these

(DOI will not work until issue is live.) DOI: http://dx.doi.org/10.2138/am.2014.4564

three suites. Dense sampling of the upper gabbros reveals a very strong compositional bimodality between the gabbros and felsic dikes. The felsic dikes can be produced as ~1-4% residual liquids of a coarse-grained parent, provided such layers later become saturated with hornblende, as is evident at the base of such dikes (Fig. 5E). Model curves are as follows: FC0 (panel B only) = fractional crystallization of a hypothetical ultramafic parent (13% MgO, 0.4% TiO_2) using mineral proportions of 50% ol + 50% cpx (D_{Ti} = 0.43; D_{Mg}=10.0); FC1 = Fractional crystallization for a GIC gabbro (sample G1A-10, Table A1; 48.9% SiO_2, 8.99% MgO, 0.18% K_2O) using mineral proportions of 7% opx + 20% cpx + 40% pl +33% hbl (D_{Si}=0.98; D_K = 0.52; D_{Ti} = 0.78; D_{Fe}=0.86; D_{Mg}=1.06). FC2 = Fractional crystallization of a GIC gabbro (sample G1A11B, Table A1; 54.2% SiO_2, 7.6% MgO, 0.24% K_2O) using mineral proportions of 13% cpx + 17% opx + 70% pl (D_{Si}=1.06; D_K=0.74; D_{Ti}=0.03; D_{Fe}=0.37; D_{Mg}=1.6). FC3 = Fractional crystallization of a GIC gabbro (sample G1A-6, Table A1; 53.6% SiO_2, 6.7% MgO, 0.2% K_2O) using mineral proportions of 20% cpx + 10% opx + 47% pl + 22% hbl + 1% ilm (D_{Si}=0.90; D_K=0.84; D_{Ti}=1.66; D_{Fe}=1.57; D_{Mg}=1.92). Models FC1 to FC3 are presumed to take place within the GIC; FC0 is presumed to occur at the base of the crust.

Figure 7. Harker variation diagrams of SiO_2 vs. Na_2O (A); MgO (B); CaO (C); Al_2O_3 (D); TiO_2 (E); Fe_2O_3t (Fe total as Fe_2O_3) (F); K_2O (G); and P_2O_5 (H) for Mingled Zone compositions. These panels compare Mingled Zone mafic enclave and felsic host compositions to one another to the Gabbro units (gray circles; Fig. 6). Except for having slightly elevated K_2O, mafic enclaves of the Mingled Zone are identical in composition to the structurally lower Gabbro unit. Felsic host materials in the Mingled Zone are roughly

(DOI will not work until issue is live.) DOI: http://dx.doi.org/10.2138/am.2014.4564

similar to the felsic dikes found in the Gabbro units with respect to most major oxides, but are still distinct, having higher Fe_2O_3t and TiO_2, and slightly higher P_2O_5 (and less scattered Na_2O and K_2O). Felsic host materials do not lie on a mixing trend with mafic enclaves. Analysis of individual enclaves indicates no zoning (rims are compositionally identical to cores) and no compositional gradients within host moving away from an enclave/host contact. FC4 = fractional crystallization of a gabbro (sample JC_H6_bot, Table A1; 51.8% SiO_2, 7.4% MgO, 0.8% K_2O) using mineral proportions of 88% hbl + 10% pl + 2% ilm (D_{Si}=0.80; D_{Ti}=1.7; D_{Al}=0.67; D_{Fe}=2.1; D_{Mg}=2.6; D_{Ca}=1.2; D_{Na}=0.52; D_K=0.46; D_P=0.33). FC5 = fractional crystallization of the same gabbro as in FC4, with mineral proportions of 5% cpx + 5% opx + 25% hbl + 64.4% pl + 0.01% ap + 0.05% ilm (D_{Si}=0.92; D_{Ti}=0.53; D_{Al}=1.4; D_{Fe}=0.75; D_{Mg}=1.01; D_{Ca}=1.6; D_{Na}=0.67; D_K=0.26; D_P=0.33. FC6 = fractional crystallization of a composite intermediate magma, similar to high SiO_2 Meladiorites MDJC-2E, -3C, -3E (59% SiO_2, 2.2% MgO, 1.2% K_2O) using mineral proportions of 14% hbl + 51.9% pl + 10% cpx + 15% opx + 2% bt +3% ilm + 3.5% titanite + 0.06% ap (D_{Si}=0.90; D_{Ti}=1.6; D_{Al}=1.1; D_{Fe}=1.6; D_{Mg}=2.1; D_{Ca}=1.9; D_{Na}=1.2; D_K=0.43; D_P=1.97).

Figure 8. A: Sub-parallel mafic intrusions, injected into a granitic host, four of which are indicated by white dashed boundaries; Cin-Ty Lee for scale. The second intrusive layer from the top has sharp contacts with granitic host both above and below, but segues into tightly disaggregated layers of rounded mafic enclaves at upper right and lower left ends. Other layers consist entirely of disaggregated mafic enclaves. These features are best

explained as flow-like structures at various stages: layers of disaggregated enclaves represent flow-front instabilities, where flow fronts first divide into fingers, and then break up into enclaves (Snyder and Tait 1995). Sharp boundaries represent flowage before flow-front instabilities take place. B: close-up view of a rounded, fine-grained mafic enclave, immediately encompassed by a fine- to medium-grained granitic host that is itself injected back into the enclave. These features show that mafic and felsic materials were both in the magmatic state at the time of injection.

Figure 9. Harker variation diagrams of SiO_2 vs. Na_2O (A); MgO (B); CaO (C); Al_2O_3 (D); TiO_2 (E); Fe_2O_3t (Fe total as Fe_2O_3) (F); K_2O (G); and P_2O_5 (H) for Mingled Zone, Granite and Granophyre map units, as well as felsic dikes from the upper Gabbro unit (Fig. 6). Gray lines shown mixing between 1) the most felsic fractionation product of Fig. 7, with 2) either Meladiorite sample MDJC-2A (solid line) or an average of Meladiorite samples MDJC-3C and -3E (dashed line); hachure marks show 10% mixing increments. Most granitic rocks show a similar span of major oxides, but Na_2O contents are very high for a given SiO_2 content for a subset of rocks from the Granite and Granophyre units (A), and these same rocks have very low K_2O (G), and show evidence of albitization. These rocks are segregated from the non-Na_2O enriched (solid black line in (A)) using Eqn. (1).

Figure 10. The Na-index (Eqn. 1) is compared to (A) K_2O contents for the granitic samples from throughout the GIC (Fig. 9), and (B) Longitude, for Granite and Granophyre samples (providing a cross section of these units). Rocks enriched in Na_2O at

a given SiO_2 content, i.e., those with a positive Na-index, have Na contents that are inversely correlated with K_2O, as opposed to those rocks with a negative Na-index, where Na and K are positively correlated. Maximum Na-indices are clearly highest at the most shallow structural levels (to the east), and decrease towards the bottom of the GIC. Rocks with a positive Na-index appear to be affected by shallow-level hydrothermal albitization (Kaur et al. 2012), with seawater as the most likely carrier of high Na_2O/K_2O ratios.

Figure 11. Rb-Sr isochron diagram for various rocks from the GIC, and a gabbro from the Hornitos pluton. All granitic rocks with low K_2O (<1 wt. %) are suspected of being albitized and so are excluded from the regression lines shown in the figure. All GIC samples fall on a single isochron that yields an age of 151.4 ± 5 Ma. If the Hornitos samples are added to the regression, the age is 151.0±5 Ma. If the one low-K granitic sample (G 13.5) that appears to fall near the isochron is added to either regression, then the sample age dates are 153 Ma, with similar errors. These age dates match those (151-153 Ma) derived from zircon studies (Saleeby et al. 1989; Ernst et al., 2009). The isochron yields a mid-ocean ridge-like initial $^{87}Sr/^{86}Sr$ of 0.7036.

Figure 12. Pseudo-ternary Quartz – Albite – Orthoclase (Q-Ab-Or), for granitic rocks (with >63% SiO_2) from the Tuolumne Igneous Complex (TIC), the Bass Lake Tonalite (BLT) and the Guadalupe Igneous Complex (GIC). Solid curves show set of liquid compositions in equilibrium quartz and an alkali feldspar, at pressures of 0.1, 50 and 200 MPa. The 1000 MPa curves show the cotectic curves for liquids precipitating Q, Ab, or Or; curves are from Blundy and Cashman (2001).

Figure 13. (A) A comparison of GIC igneous rock compositions to the enclosing Mariposa Formation sediments, the latter of which are displaced to much higher ASI or alumina saturation indices (molar ratio: Al_2O_3/[CaO – 1.67(P_2O_5) + Na_2O + K_2O]) (Chappell, 1999) vs. wt. % SiO_2. Felsic granites and intermediate composition enclaves (gray triangles with <65% SiO_2) from the Granite units are plotted. GIC samples have ASI values that are too low to allow much of any assimilation of Mariposa Formation sediments. (B) GIC samples also have P_2O5/TiO_2 ratios that are much lower at a given SiO_2 content compared to metavolcanic rocks from the region, which are expected to comprise the lower crust. A small subset (~12%) of granitic GIC samples is plausible partial melts of metavolcanic materials, but the vast majority must be produced by some other mechanism. (C) A comparison of FeOt (=0.9[Fe_2O_3]) vs. Na2O + K2O + P2O5 + TiO2, as a test for liquid immiscibility. Solid lines (Charlier and Grove 2012) separate fields where liquids are immiscible (upper right) or miscible (lower left), which vary in position as a function of SiO_2 content (curves for 50 and 60 wt. % SiO_2 are shown). All GIC samples plot in the miscible field, regardless of SiO_2 content.

Figure 14. SiO_2 vs. (A) Na_2O (filtered using Eqn. 1) and (B) Al_2O_3 for mafic-intermediate and granitic samples from the GIC. Mafic and intermediate enclaves from the Granite and Granophyre units appear as gray triangles with SiO_2< 65 wt. %, Hexagons represent calculated intermediate liquids determined by mass balance with averages of Meladiorites or Mingled Zone rocks with 50-55% SiO_2, or Meladiorites with 50-52% SiO_2; these lines meet at the common felsic end-member (75.6% SiO_2; Table 1),

generated at melt fractions of 25-55%, depending upon assumed residual mafic assemblage. None of these curves reproduces the observed trend of granitic samples, but several GIC samples in the range 60-66% SiO_2 approach putative intermediate parent liquid compositions (hexagons). Curves FC7 and FC8 represent plagioclase- and amphibole-rich fractional crystallization curves respectively, using a gabbro with 7.44% MgO as a parent magma (sample JC_H6_bot; Table A1; hachure marks indicate 10% increments in *F*. FC7 = 67.9% hbl + 30% pl + 0.1% ap + 2% mt; D_{Si}=0.83; D_{Na} = 0.60; D_{Al} = 0.96. FC8 = 50% hbl + 39.4% pl + 5% cpx + 5% opx + 0.1% ap + 0.05% mt; D_{Si}=0.88; D_{Na} = 0.59; D_{Al} = 1.06. Dashed blue line indicates mixing between the felsic end-member magma (75.6% SiO_2) and a putative mafic-intermediate magma generated by a composite of FC7 and FC8.

Figure 15. Model for assembly of a pluton. Diagram is schematic and is intended to indicate processes, not scale. Dark region at the base are Gabbro unit. Dark gray colors above represent mafic-intermediates. Light gray colors are granitic magmas, which occurs as discrete dikes in the gabbros, but amalgamate to form larger pods in the Meladiorite and Mingled Zone. Larger dikes and pods at the top of the Meladiorite and Mingled Zone have sufficient buoyancy to rise upwards and add new mass to the growing felsic cap. The felsic cap is a convective body (dashed arrows); flow is arrested at the top of the pluton, where high undercoolings allow the development of granophyric intergrowth textures.

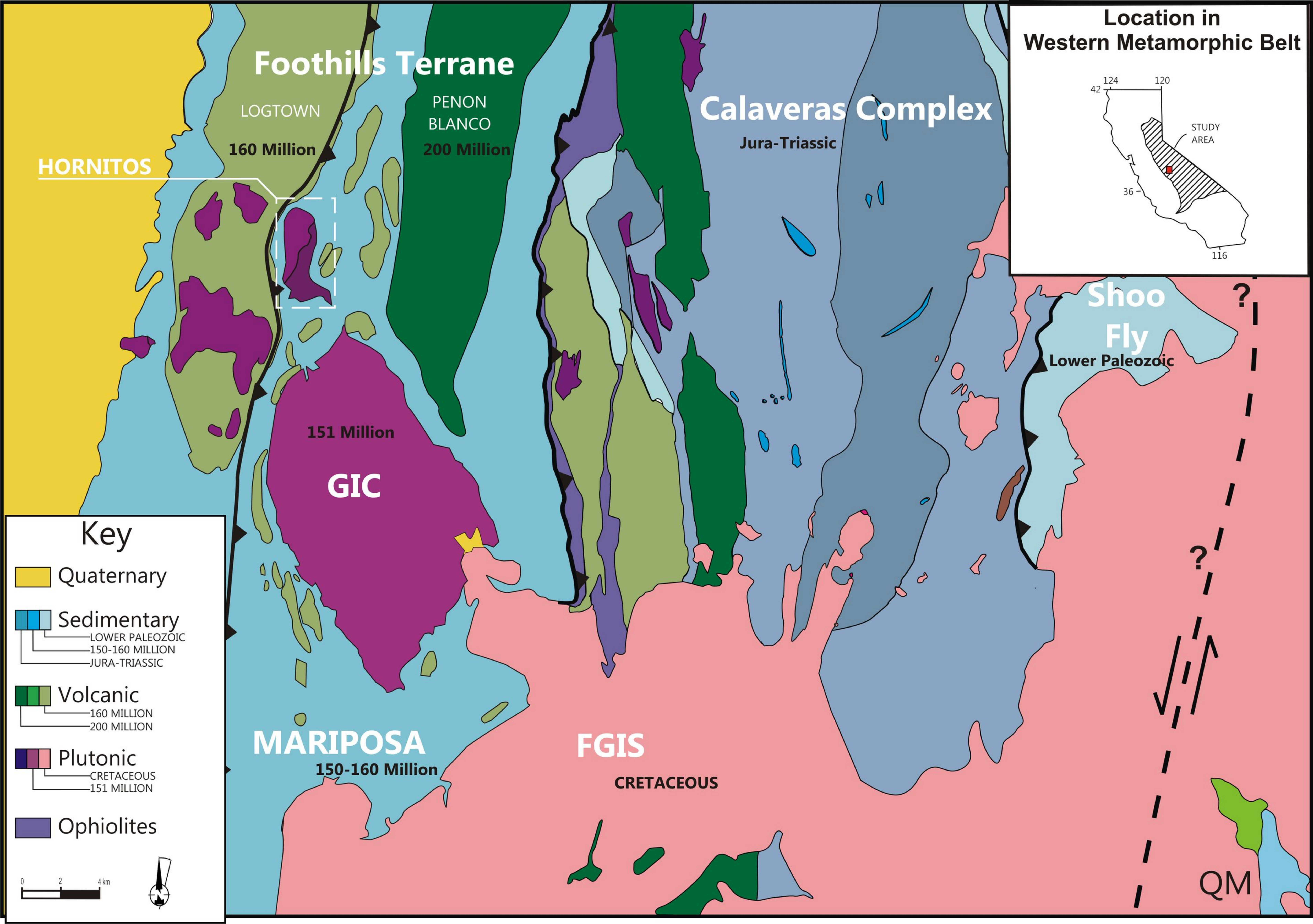

Foothills Terrane
LOGTOWN
160 Million
PENON
BLANCO
200 Million
HORNITOS
Calaveras Complex
Jura-Triassic
Location in
Western Metamorphic Belt
124
120
42
STUDY
AREA
36
116
Shoo
Fly
Lower Paleozoic
?
?
151 Million
GIC
MARIPOSA
150-160 Million
FGIS
CRETACEOUS
QM
Key
Quaternary
Sedimentary
LOWER PALEOZOIC
150-160 MILLION
JURA-TRIASSIC
Volcanic
160 MILLION
200 MILLION
Plutonic
CRETACEOUS
151 MILLION
Ophiolites
0
2
4 km

Figure 2

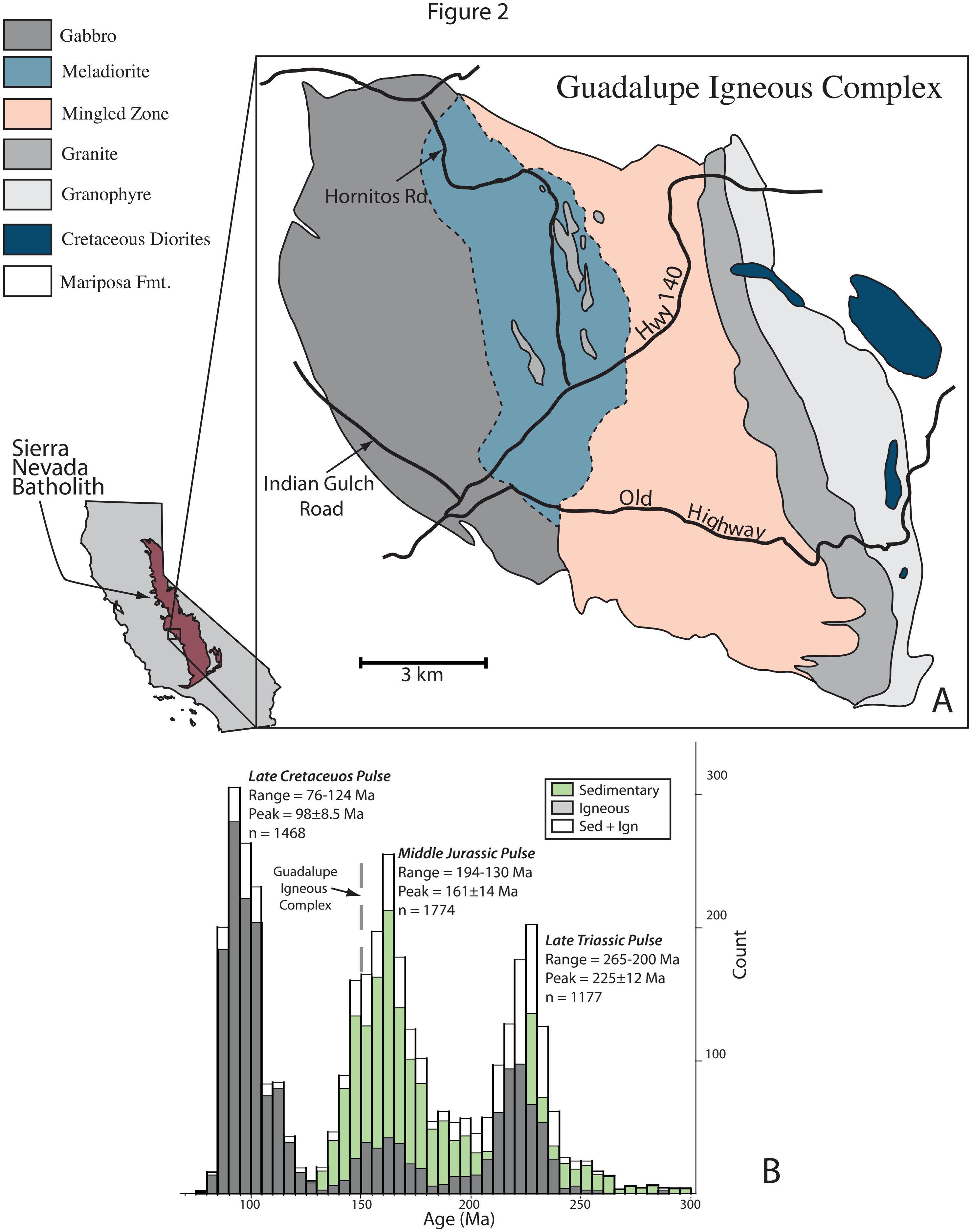

Gabbro
Meladiorite
Mingled Zone
Granite
Granophyre
Cretaceous Diorites
Mariposa Fmt.
Guadalupe Igneous Complex
Hornitos Rd.
Hwy 140
Indian Gulch Road
Old Highway
Sierra Nevada Batholith
3 km
A
Late Cretaceuos Pulse
Range = 76-124 Ma
Peak = 98±8.5 Ma
n = 1468
Sedimentary
Igneous
Sed + Ign
Guadalupe Igneous Complex
Middle Jurassic Pulse
Range = 194-130 Ma
Peak = 161±14 Ma
n = 1774
Late Triassic Pulse
Range = 265-200 Ma
Peak = 225±12 Ma
n = 1177
300
200
100
Count
100
150
200
250
300
Age (Ma)
B

Figure 3

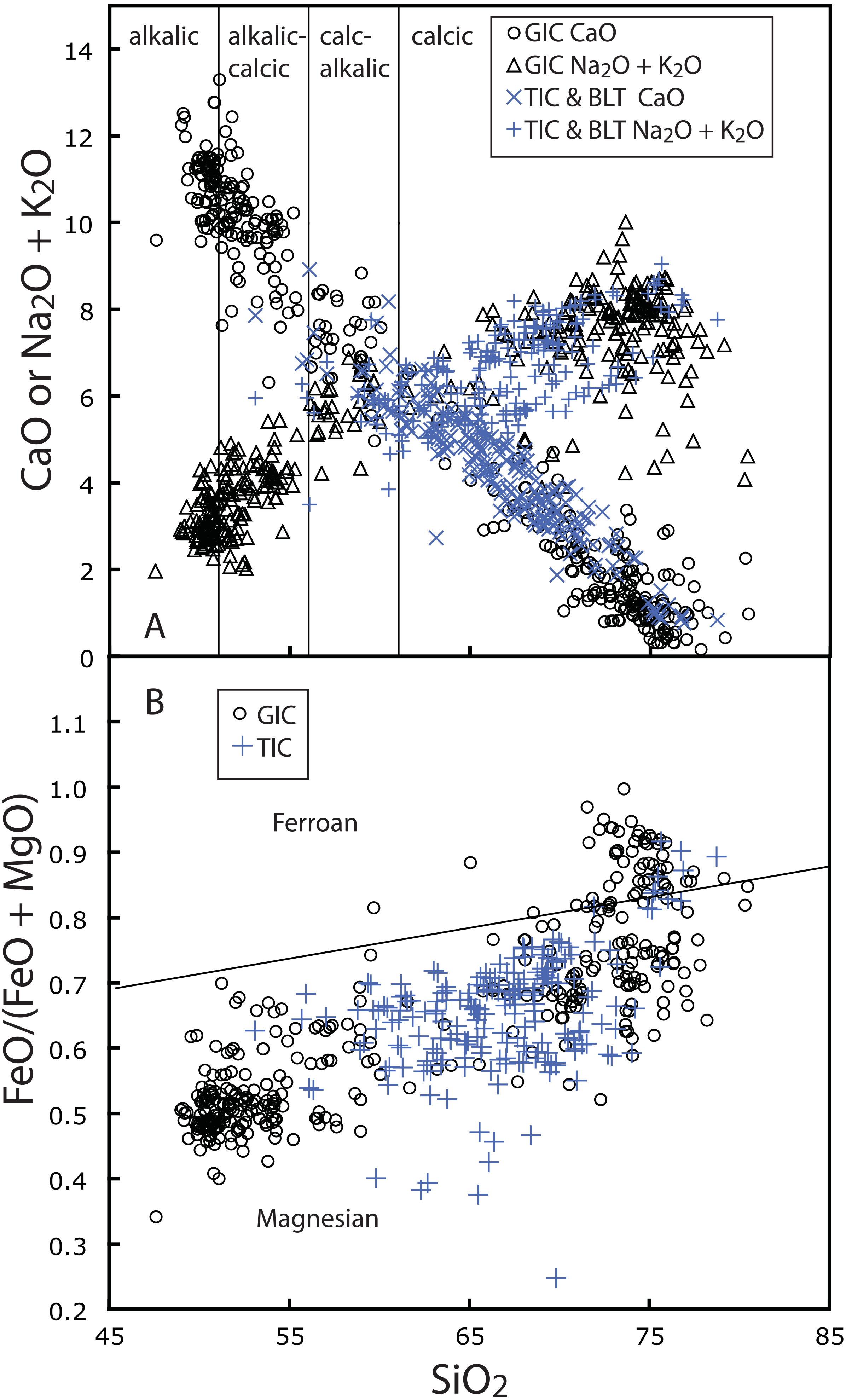

alkalic
alkalic-calcic
calc-alkalic
calcic
GIC CaO
GIC $Na_2O + K_2O$
TIC & BLT CaO
TIC & BLT $Na_2O + K_2O$
CaO or $Na_2O + K_2O$
A
B
GIC
TIC
Ferroan
Magnesian
FeO/(FeO + MgO)
SiO_2

Figure 3

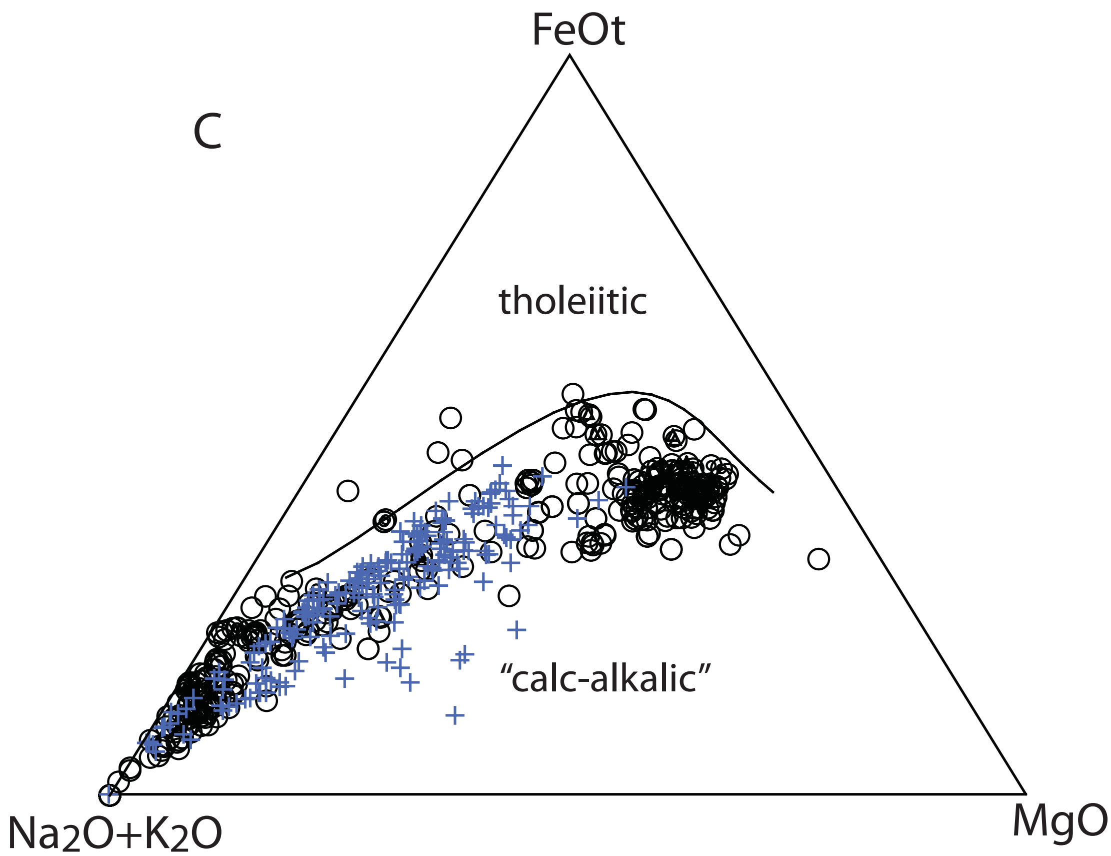

FeOt
C
tholeiitic
"calc-alkalic"
Na2O+K2O
MgO

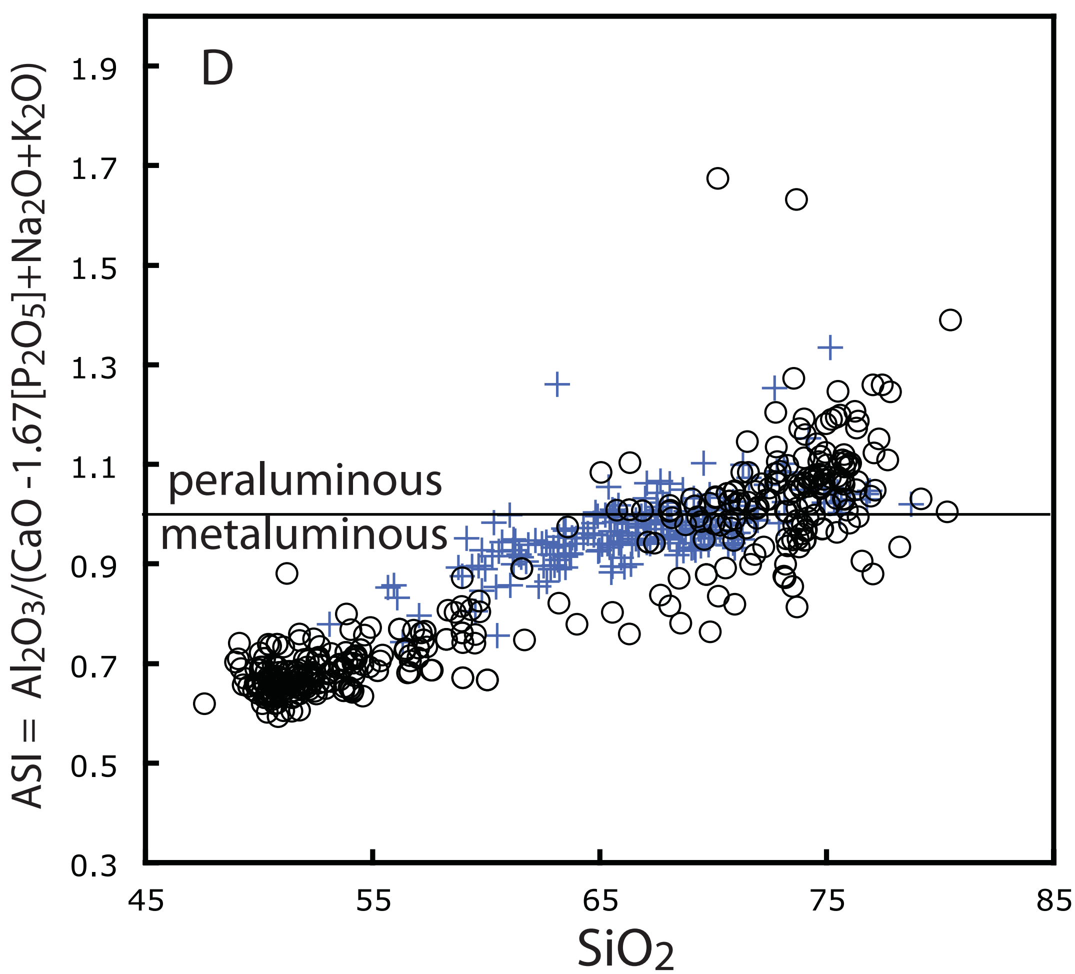

D
1.9
1.7
1.5
1.3
1.1
0.9
0.7
0.5
0.3
peraluminous
metaluminous
ASI = Al2O3/(CaO -1.67[P2O5]+Na2O+K2O)
45
55
65
75
85
SiO2

Figure 4

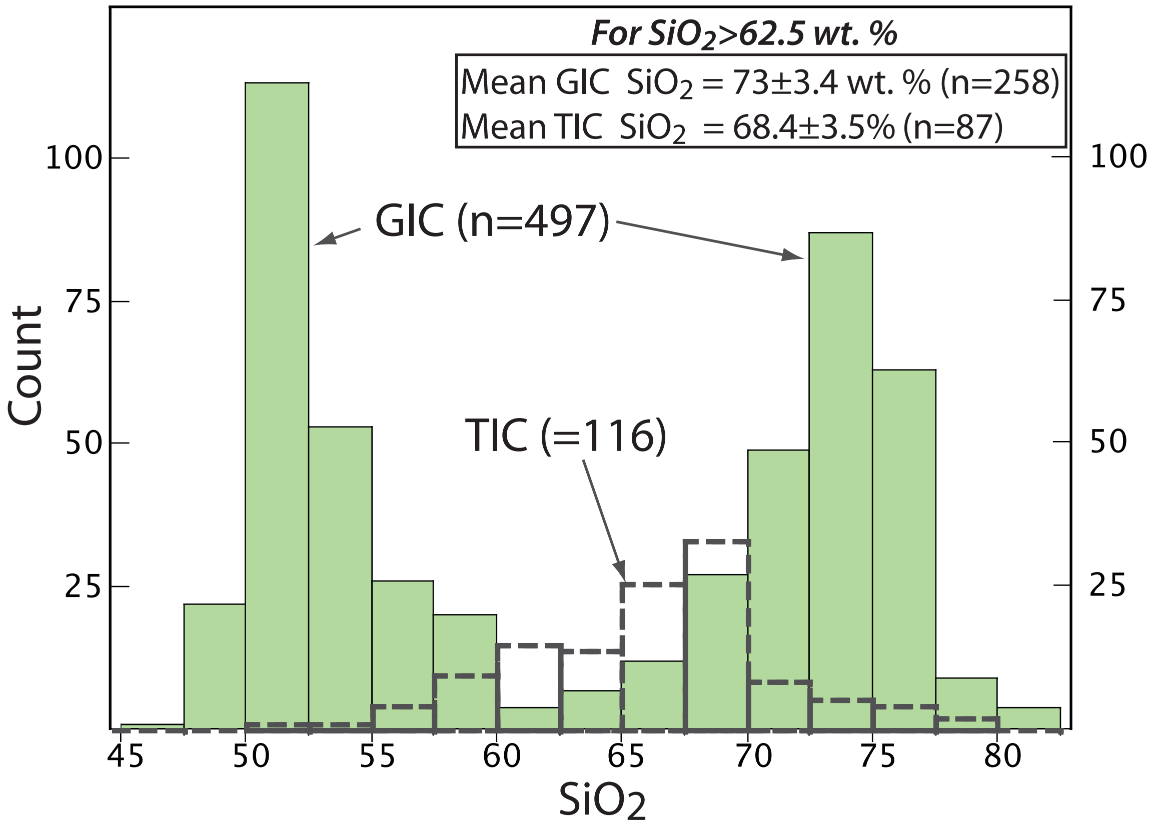

For SiO2>62.5 wt. %
Mean GIC SiO2 = 73±3.4 wt. % (n=258)
Mean TIC SiO2 = 68.4±3.5% (n=87)
GIC (n=497)
TIC (=116)
Count
100
75
50
25
45
50
55
60
65
70
75
80
SiO2

Figure 5A - C

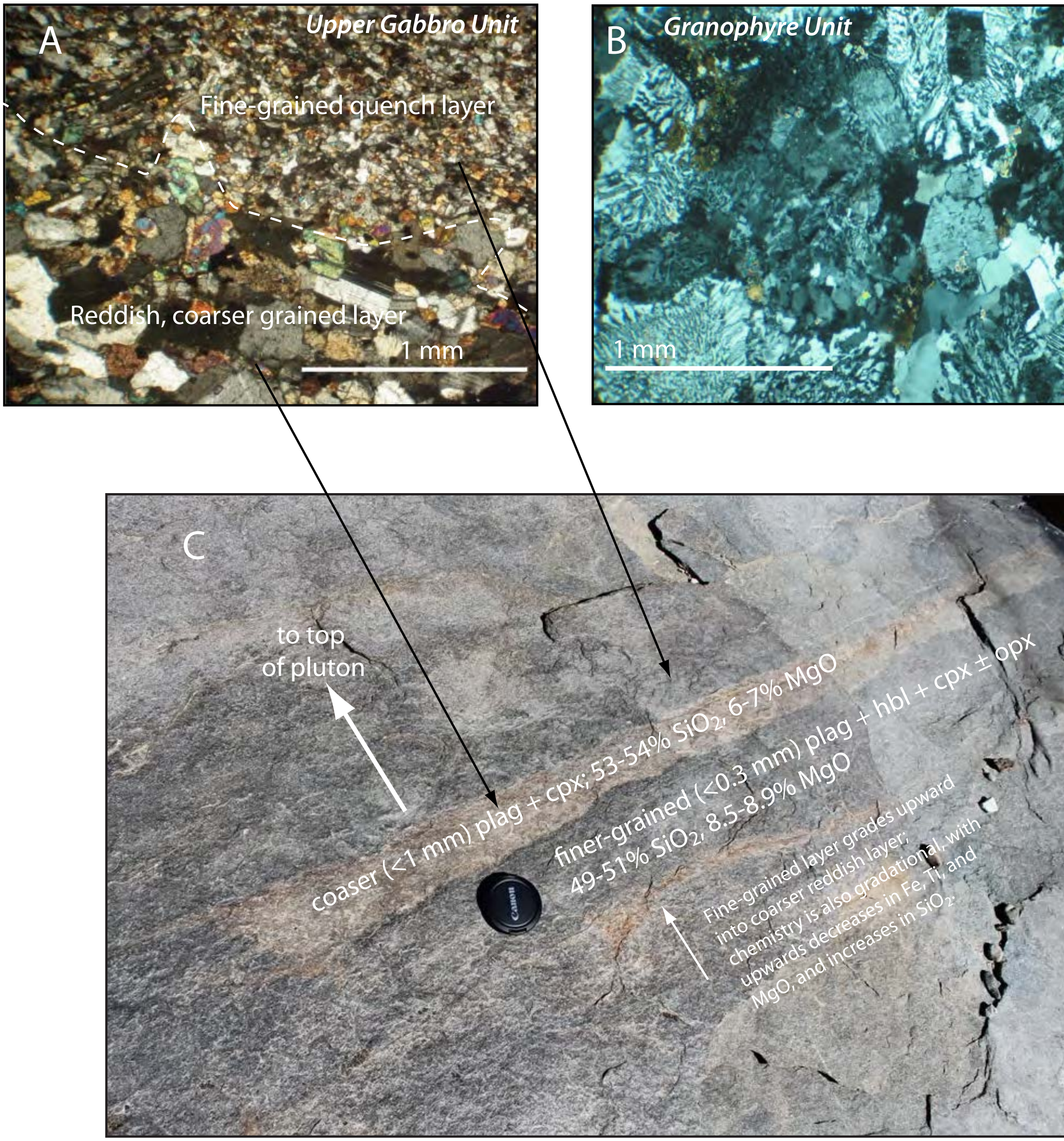
A
Upper Gabbro Unit
Fine-grained quench layer
Reddish, coarser grained layer
1 mm
B
Granophyre Unit
1 mm
C
to top
of pluton
coaser (<1 mm) plag + cpx; 53-54% SiO2, 6-7% MgO
finer-grained (<0.3 mm) plag + hbl + cpx ± opx
49-51% SiO2, 8.5-8.9% MgO
Fine-grained layer grades upward
into coarser reddish layer;
chemistry is also gradational, with
upwards decreases in Fe, Ti, and
MgO, and increases in SiO2.

Figures 5D-E

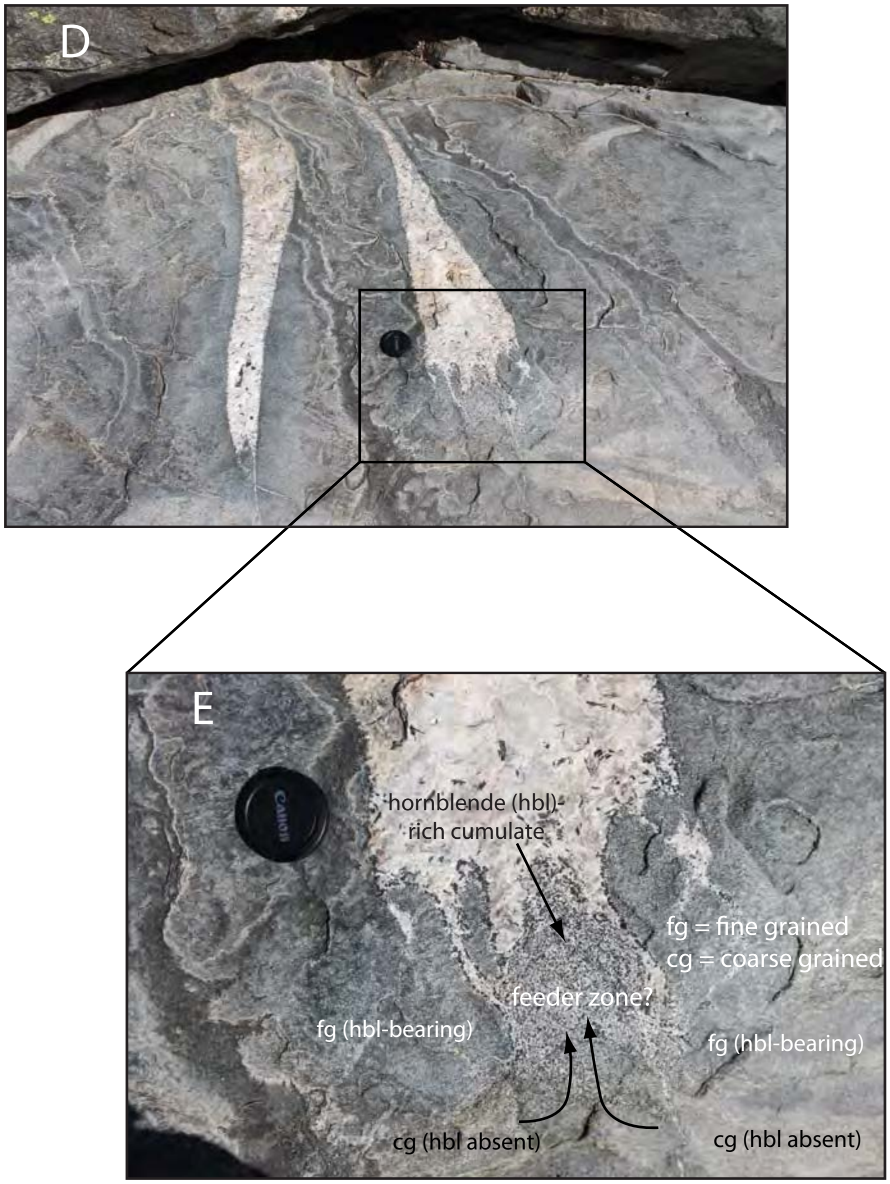
D
E
hornblende (hbl)
rich cumulate
fg = fine grained
cg = coarse grained
feeder zone?
fg (hbl-bearing)
fg (hbl-bearing)
cg (hbl absent)
cg (hbl absent)

Figure 6

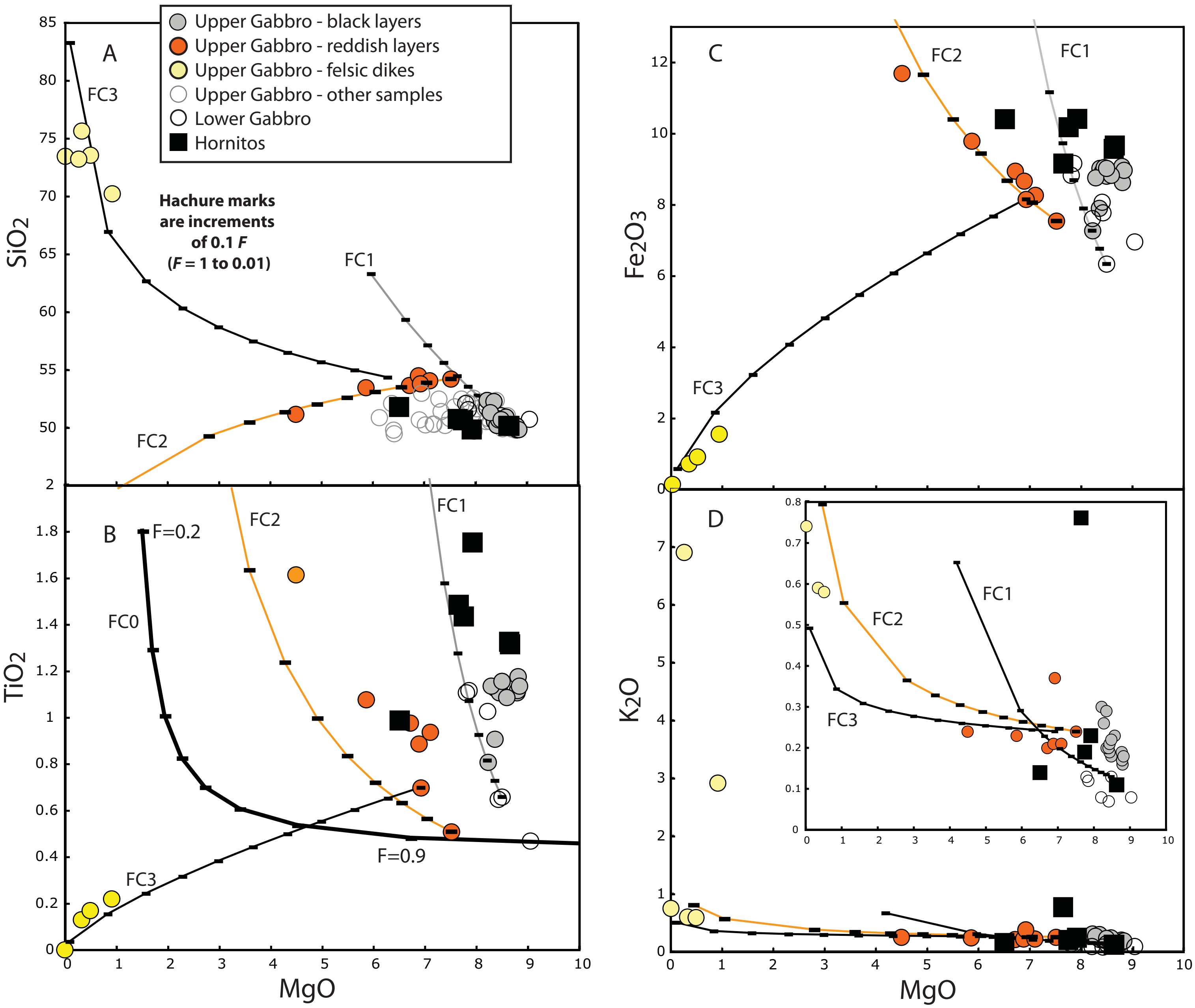

Upper Gabbro - black layers
Upper Gabbro - reddish layers
Upper Gabbro - felsic dikes
Upper Gabbro - other samples
Lower Gabbro
Hornitos
Hachure marks are increments of 0.1 F (F = 1 to 0.01)
A
B
C
D
FC0
FC1
FC2
FC3
F=0.2
F=0.9
SiO2
TiO2
Fe2O3
K2O
MgO

Figure 7 A-D

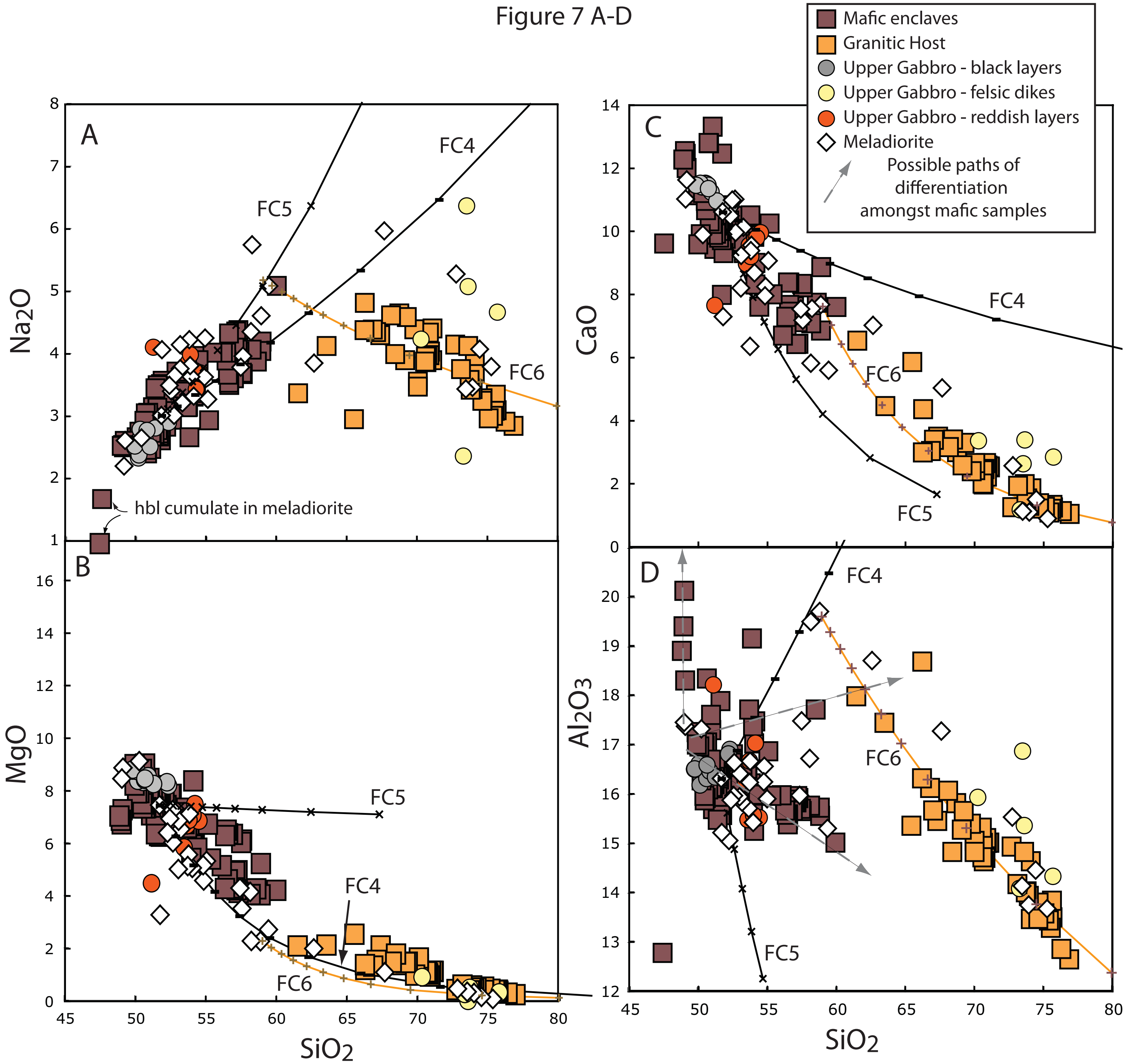
Mafic enclaves
Granitic Host
Upper Gabbro - black layers
Upper Gabbro - felsic dikes
Upper Gabbro - reddish layers
Meladiorite
Possible paths of differentiation amongst mafic samples
A
B
C
D
FC4
FC5
FC6
hbl cumulate in meladiorite
Na_2O
MgO
CaO
Al_2O_3
SiO_2

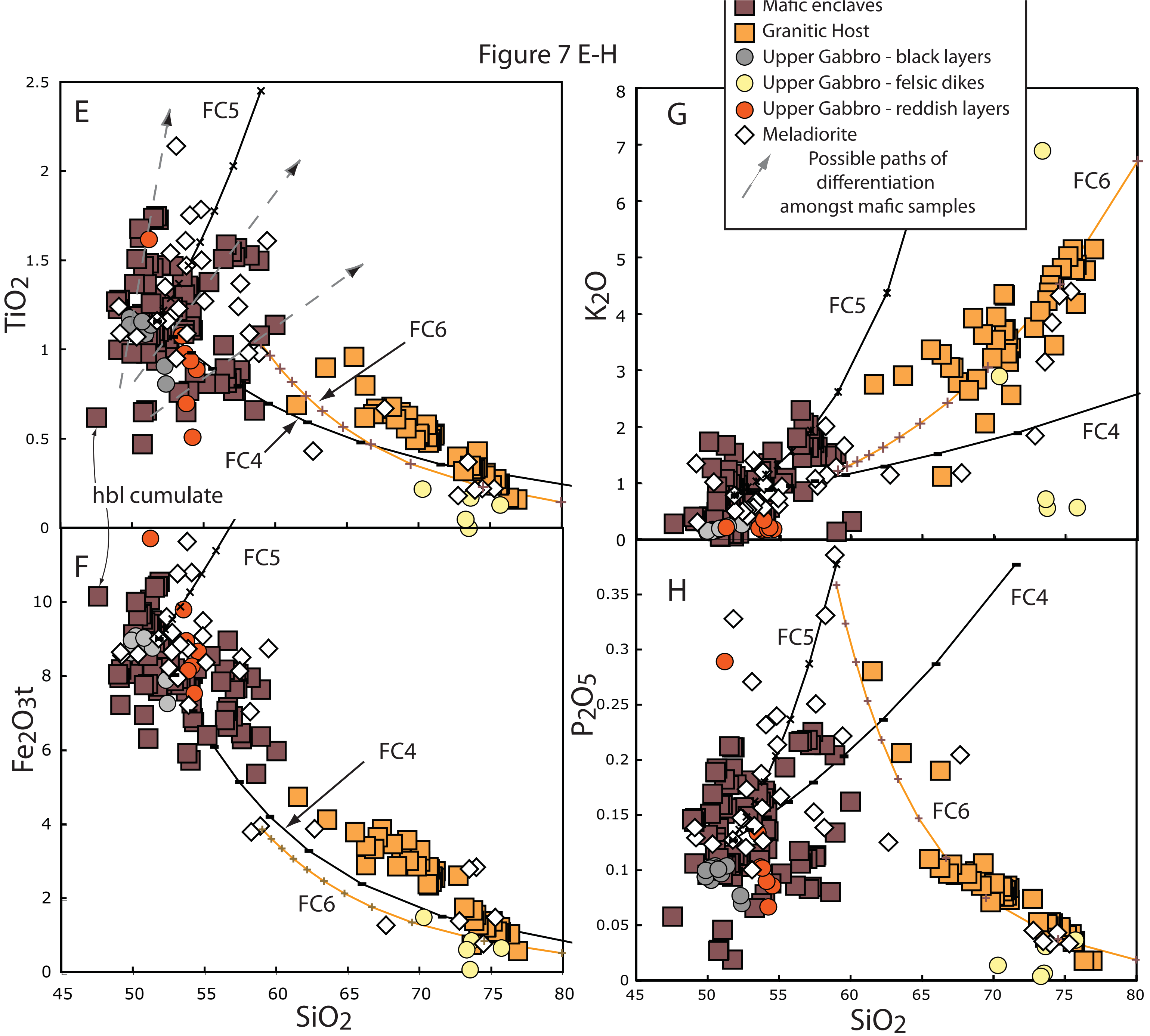

Figure 7 E-H
Mafic enclaves
Granitic Host
Upper Gabbro - black layers
Upper Gabbro - felsic dikes
Upper Gabbro - reddish layers
Meladiorite
Possible paths of differentiation amongst mafic samples
E
F
G
H
FC4
FC5
FC6
hbl cumulate
TiO2
Fe2O3t
K2O
P2O5
SiO2

Figure 8


A
parallel mafic intrusions into host granitic magma
B
20 cm

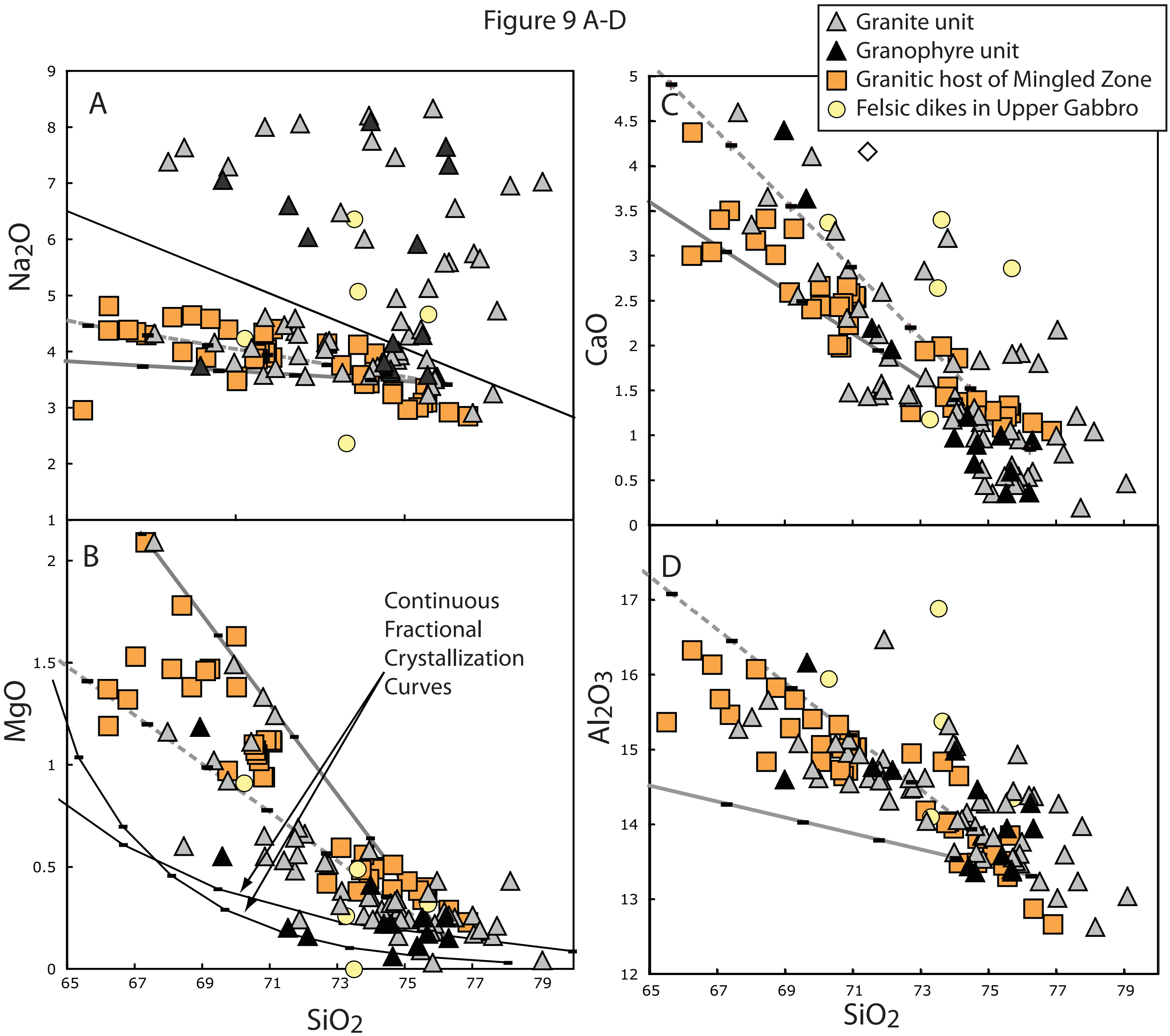

Figure 9 A-D
Granite unit
Granophyre unit
Granitic host of Mingled Zone
Felsic dikes in Upper Gabbro
A
B
C
D
Na_2O
MgO
CaO
Al_2O_3
SiO_2
SiO_2
Continuous Fractional Crystallization Curves

Figure 9 E-H

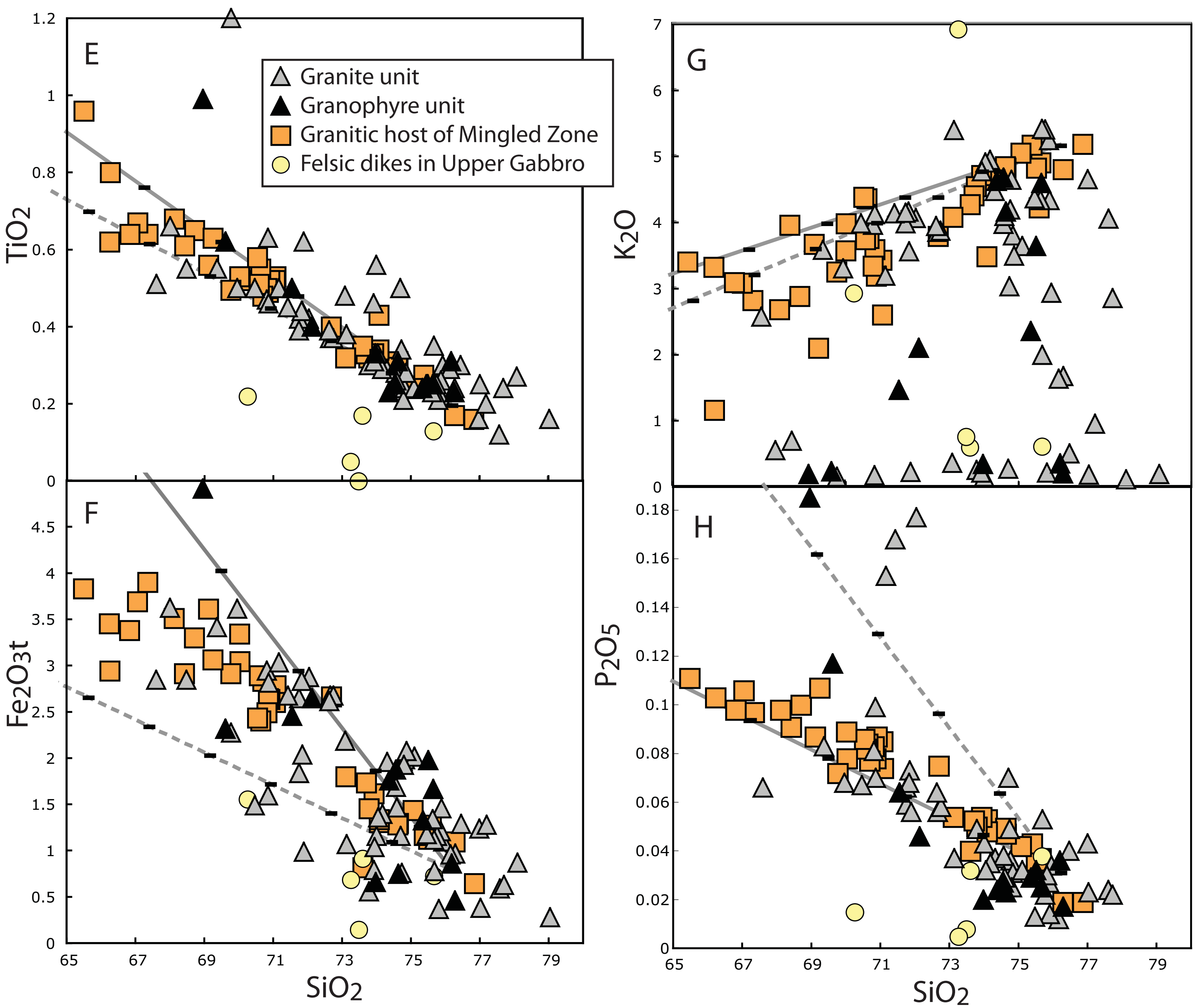

E
F
G
H
Granite unit
Granophyre unit
Granitic host of Mingled Zone
Felsic dikes in Upper Gabbro
TiO_2
Fe_2O_3t
K_2O
P_2O_5
SiO_2
SiO_2

Figure 10

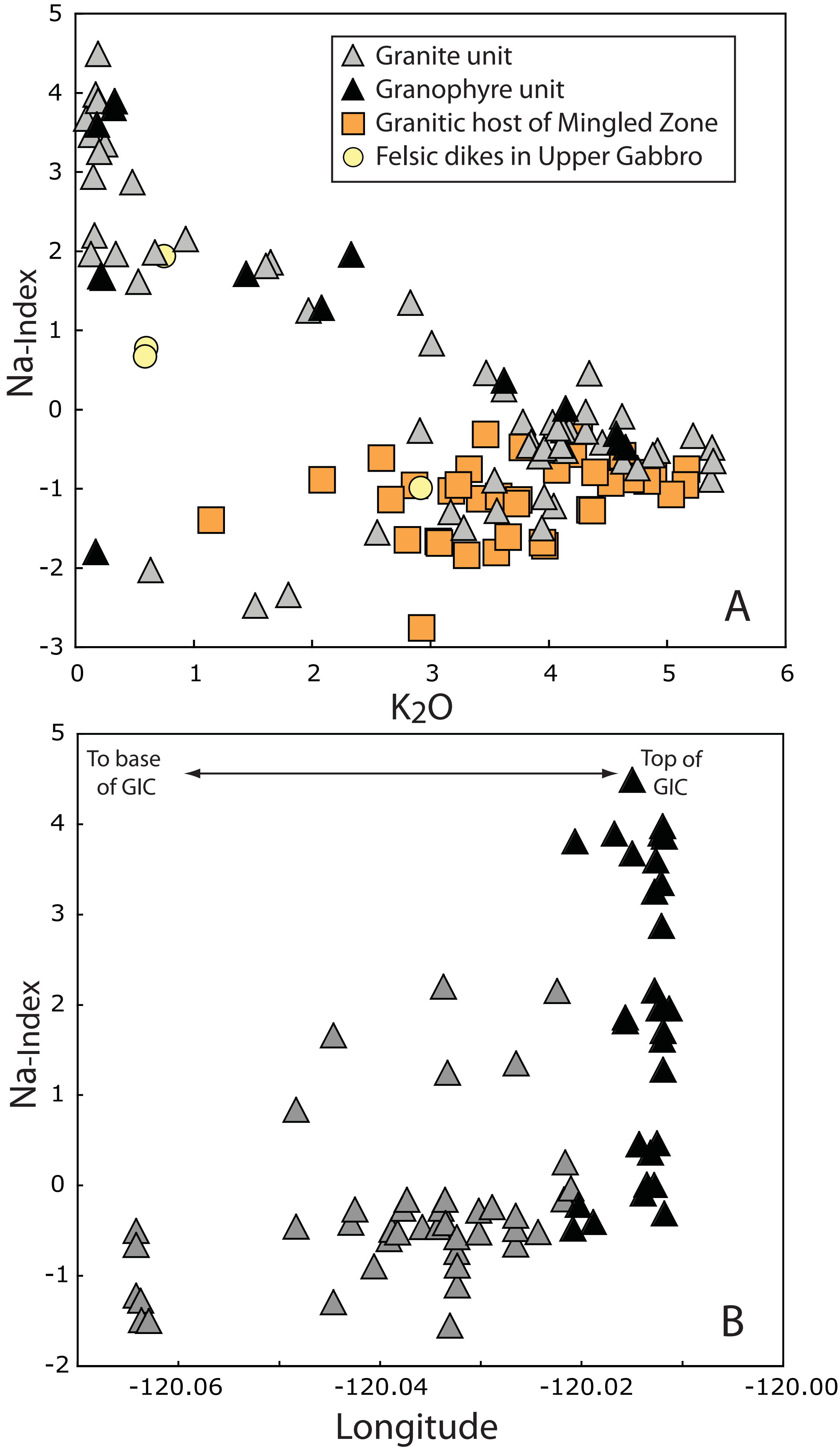

Granite unit
Granophyre unit
Granitic host of Mingled Zone
Felsic dikes in Upper Gabbro
Na-Index
5
4
3
2
1
0
-1
-2
-3
0
1
2
3
4
5
6
K_2O
A
To base of GIC
Top of GIC
Na-Index
-2
-120.06
-120.04
-120.02
-120.00
Longitude
B

Figure 11

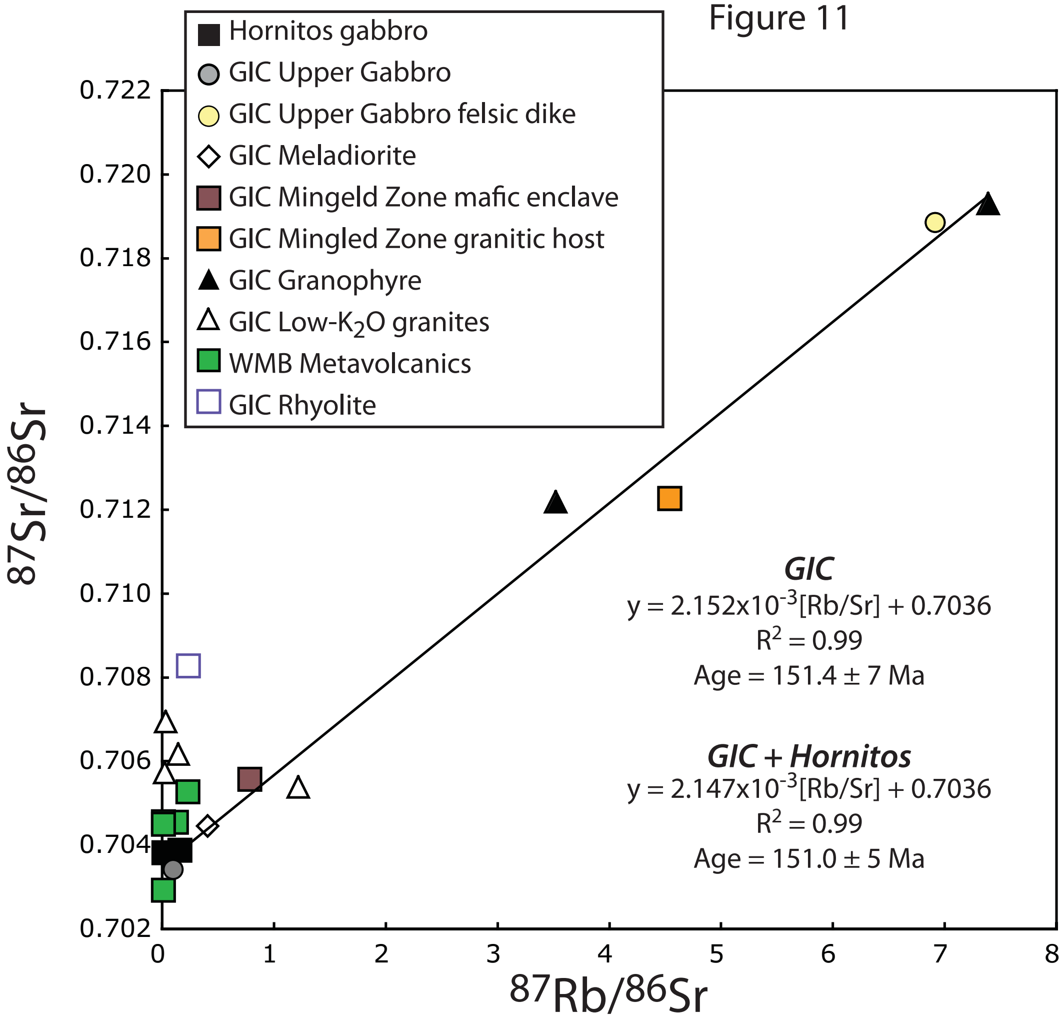
Hornitos gabbro
GIC Upper Gabbro
GIC Upper Gabbro felsic dike
GIC Meladiorite
GIC Mingeld Zone mafic enclave
GIC Mingled Zone granitic host
GIC Granophyre
GIC Low-K_2O granites
WMB Metavolcanics
GIC Rhyolite
GIC
y = 2.152x10^{-3}[Rb/Sr] + 0.7036
R^2 = 0.99
Age = 151.4 ± 7 Ma
GIC + Hornitos
y = 2.147x10^{-3}[Rb/Sr] + 0.7036
R^2 = 0.99
Age = 151.0 ± 5 Ma
$^{87}Sr/^{86}Sr$
$^{87}Rb/^{86}Sr$
0.722
0.720
0.718
0.716
0.714
0.712
0.710
0.708
0.706
0.704
0.702
0
1
2
3
4
5
6
7
8

Figure 12

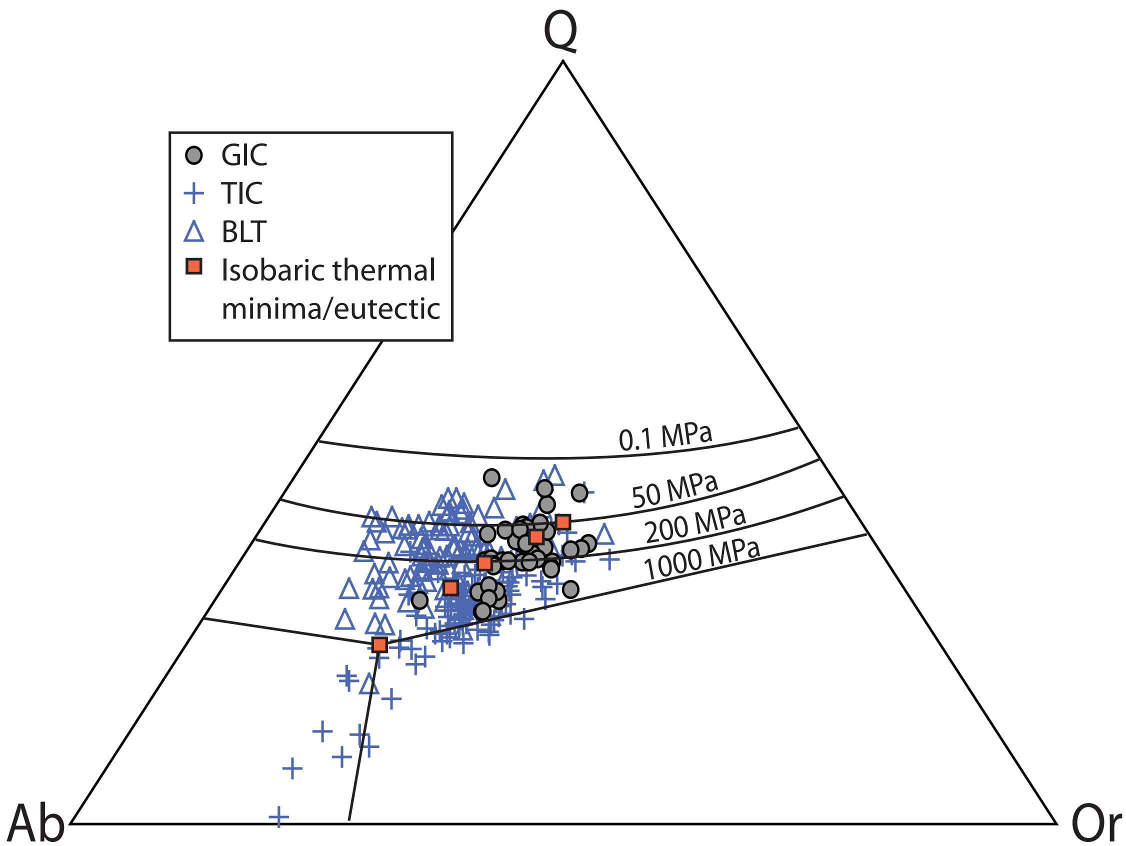

Q
GIC
TIC
BLT
Isobaric thermal minima/eutectic
0.1 MPa
50 MPa
200 MPa
1000 MPa
Ab
Or

Figure 13

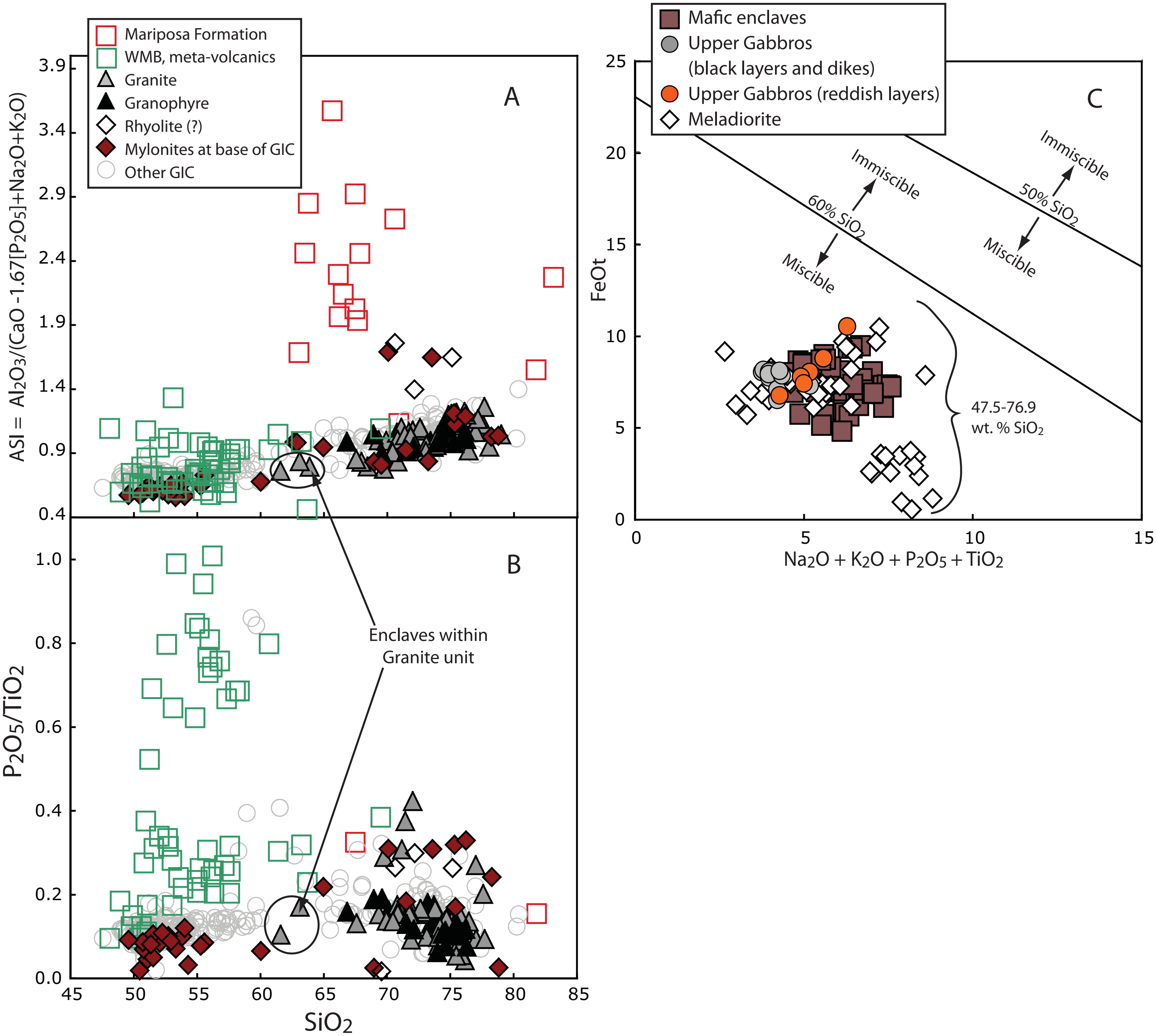

Mariposa Formation
WMB, meta-volcanics
Granite
Granophyre
Rhyolite (?)
Mylonites at base of GIC
Other GIC
A
B
ASI = $Al_2O_3/(CaO - 1.67[P_2O_5]+Na_2O+K_2O)$
P_2O_5/TiO_2
SiO_2
Enclaves within
Granite unit
Mafic enclaves
Upper Gabbros
(black layers and dikes)
Upper Gabbros (reddish layers)
Meladiorite
C
Immiscible
Miscible
60% SiO_2
50% SiO_2
47.5-76.9
wt. % SiO_2
FeOt
$Na_2O + K_2O + P_2O_5 + TiO_2$

Figure 14

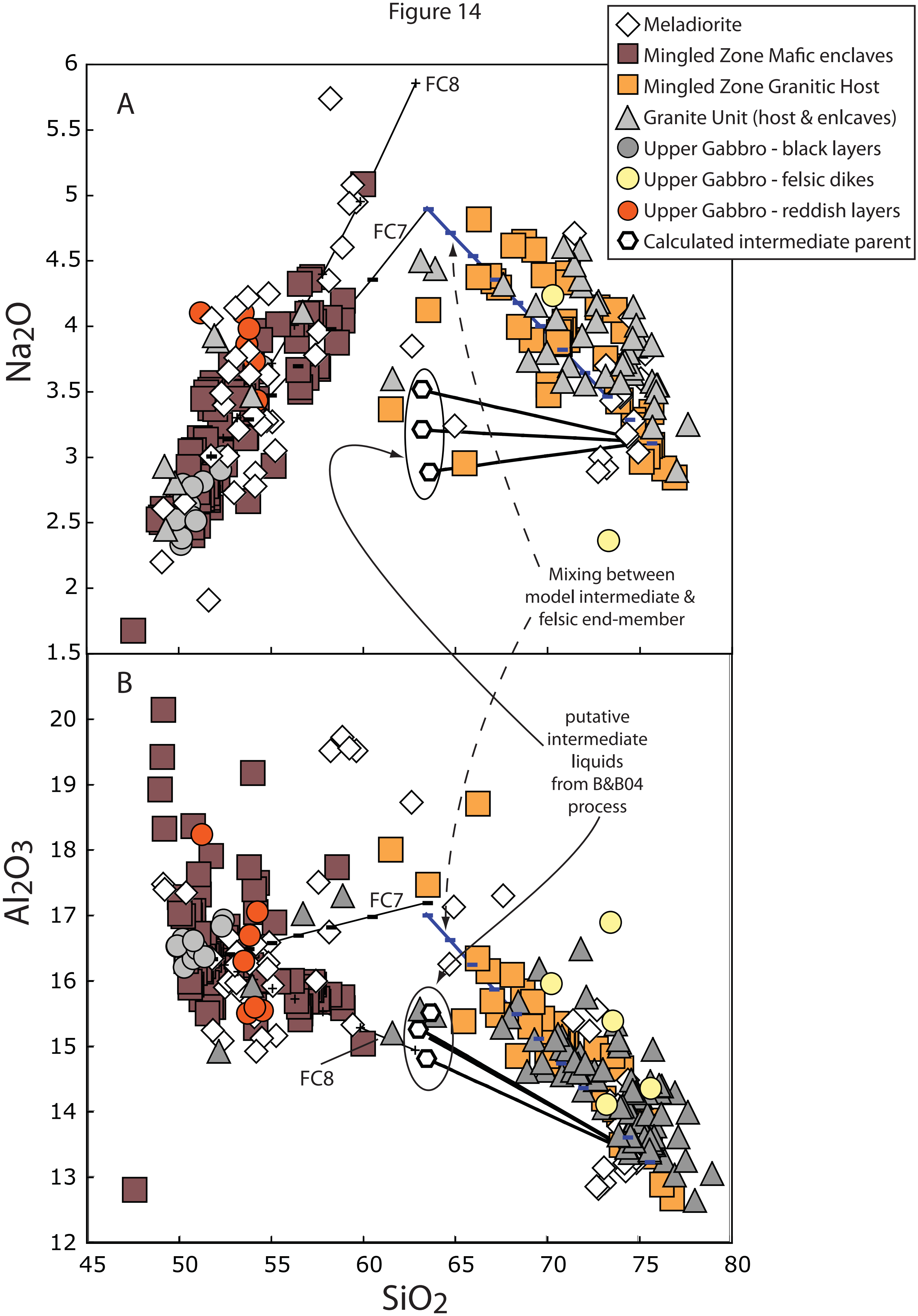
Meladiorite
Mingled Zone Mafic enclaves
Mingled Zone Granitic Host
Granite Unit (host & enlcaves)
Upper Gabbro - black layers
Upper Gabbro - felsic dikes
Upper Gabbro - reddish layers
Calculated intermediate parent
A
FC8
FC7
Mixing between model intermediate & felsic end-member
B
putative intermediate liquids from B&B04 process
FC7
FC8
Na_2O
Al_2O_3
SiO_2
6
5.5
5
4.5
4
3.5
3
2.5
2
1.5
20
19
18
17
16
15
14
13
12
45
50
55
60
65
70
75
80

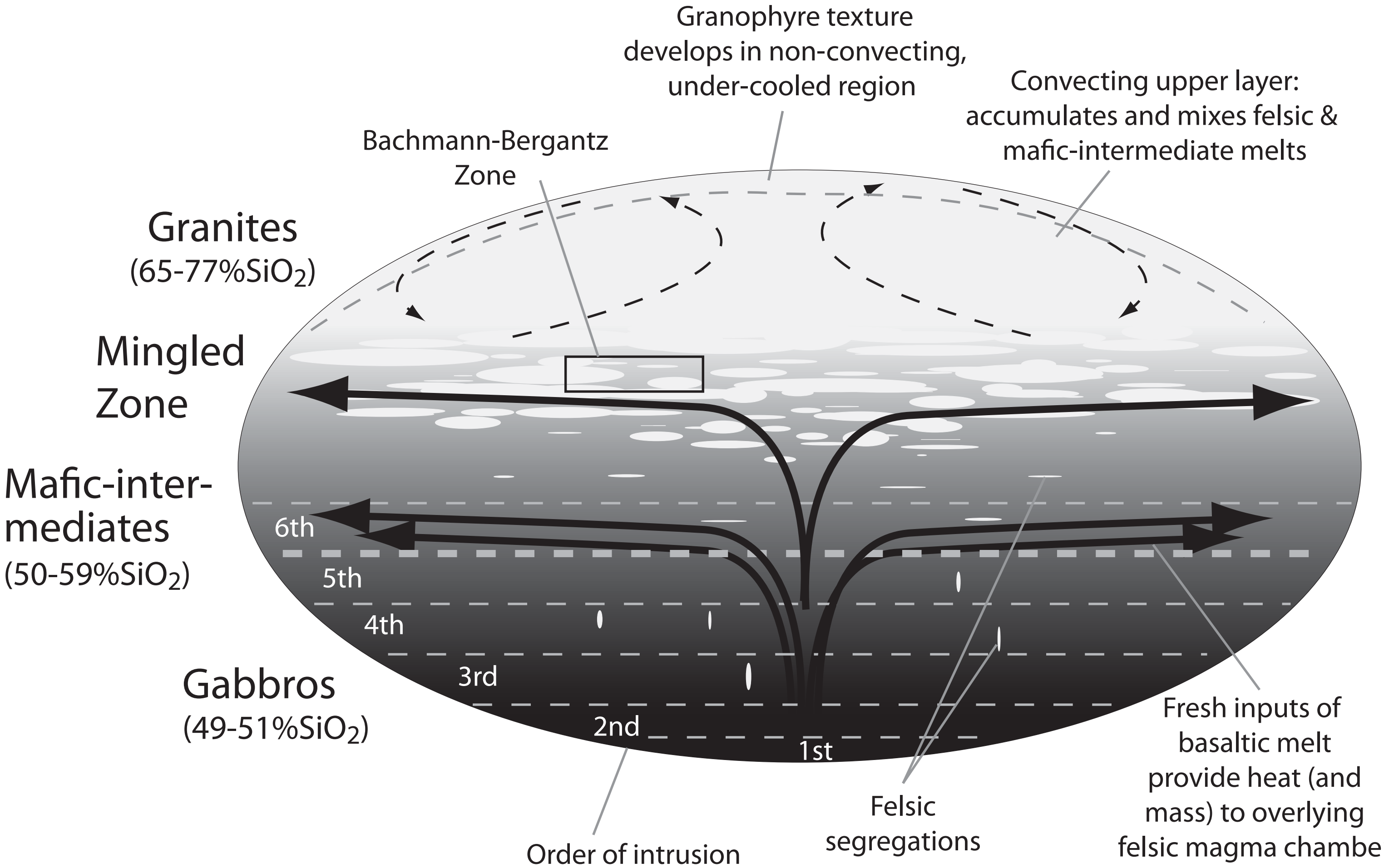
Granophyre texture
develops in non-convecting,
under-cooled region
Convecting upper layer:
accumulates and mixes felsic &
mafic-intermediate melts
Bachmann-Bergantz
Zone
Granites
(65-77%SiO_2)
Mingled
Zone
Mafic-inter-
mediates
(50-59%SiO_2)
6th
5th
4th
3rd
2nd
1st
Gabbros
(49-51%SiO_2)
Fresh inputs of
basaltic melt
provide heat (and
mass) to overlying
felsic magma chamber
Felsic
segregations
Order of intrusion

Table 1. Calculated Parental and Derivative Magma Compositions, and Comparisons to Arc and Oceanic Volcanics

Primitive GIC Compositions[1]	SiO_2	TiO_2	Al_2O_3	Fe_2O_3	MnO	MgO	CaO	Na_2O	K_2O	P_2O_5	Total
GIC Lower Gabbro	50.9	0.57	17.2	6.7	0.12	8.7	13.1	2.4	0.11	0.04	99.8
GIC Upper Gabbro	49.9	1.14	16.6	8.9	0.16	8.8	11.5	2.4	0.18	0.10	99.7
GIC Meladiorite - mafic	50.4	1.13	17.1	8.3	0.17	8.8	10.9	2.7	0.62	0.13	100.1
GIC Mningled Zone - mafic enclave	50.8	1.13	16.7	9.0	0.14	8.0	10.3	2.7	0.92	0.12	99.9
GIC Granite - mafic enclave	49.3	1.30	16.8	9.0	0.19	8.6	11.2	2.7	0.47	0.08	99.6
Primitive Arc Volcanics with 8.8% MgO[2]											
Marianas (GEOROC)	50.1	0.80	16.7	9.4	0.14	8.8	10.7	2.6	0.58	0.10	100.0
Izu Bonin (Georoc)	50.0	0.43	17.3	9.0	0.15	8.8	11.9	0.4	1.52	0.13	99.8
Cascades	50.1	1.00	17.1	8.9	0.16	8.8	10.4	2.8	0.48	0.16	99.9
Aleutians	48.6	1.79	15.1	11.5	0.17	8.8	10.0	3.2	1.08	0.37	100.5
Mexican arc	50.0	1.42	15.6	9.3	0.14	8.8	8.9	3.1	1.93	0.50	99.8
Japan	47.1	2.35	16.4	10.2	0.16	8.8	8.1	3.7	1.77	0.61	99.2
Andes	49.6	1.51	15.8	10.1	0.15	8.8	9.4	3.1	1.18	0.39	99.9
Primitive Oceanic Compositions with 8.8% MgO[3]											
MORB	49.9	1.12	15.7	10.0	0.16	8.8	12.2	2.4	0.09	0.11	100.4
Mauna Loa subaerial (HSDP	49.9	2.06	14.1	12.3	0.18	8.8	10.5	1.9	0.12	0.18	100.0
Mass balance results for tests of Bachmann & Bergantz (2004) model (HC = hypothetical cumulate)[5]											
HC1 (mafic sample from Meladiorite)	49.2	1.09	17.4	8.6	0.14	8.9	11.6	2.6	0.3	0.13	99.9
Predicted intermediate magma at F=0.55	63.7	0.63	15.1	4.4	0.07	4.2	5.9	2.9	2.8	0.08	99.8
Target felsic interstitial melt composition	75.6	0.25	13.2	1.51	0.02	0.35	1.19	3.1	4.9	0.03	100.0
HC2 (Meladiorites with SiO_2<60%)	54.2	1.28	16.5	8.3	0.14	5.8	9.2	3.6	0.88	0.18	100.0
Predicted intermediate magma at F=0.45	63.8	0.82	15.0	5.0	0.08	3.4	5.6	3.4	2.7	0.11	99.9
Target felsic interstitial melt composition	75.6	0.25	13.2	1.51	0.02	0.35	1.19	3.1	4.9	0.03	100.0
HC3 (Coarse-grained Upper Gabbros)	53.9	0.85	16.1	8.6	0.16	6.8	9.6	3.8	0.24	0.1	100.1
Predicted intermediate magma at F=0.45	62.6	0.54	15.7	5.2	0.10	4.0	6.7	4.2	0.75	0.07	99.9
Target felsic interstitial melt composition	73.2	0.17	15.2	1.07	0.03	0.6	3.2	4.7	1.4	0.03	99.5

[1]Primitive GIC compositions are averages of fine-grained rocks with >8.5% MgO. [2]Primitive arc compositions are from GEOROC and represent averages of samples with 8.7-8.9% MgO. [3]Primitive oceanic compositions are from PETDB and Rhodes and Vollinger (2003), representing averages of samples with 8.7-8.8% MgO. [4]The GIC felsic end member composition is a composite of samples with 74-77% SiO_2, and K_2O>4.5%, from the Mingled Zone, Granite and Granophyre map units. [5]Intermediate composition magmas are best-fit compositions obtained by mass balance of hypothetical cumulates (HC) so as to yield the indicated felsic interstitial liquid compositions. In HC1 and HC2, the felsic interstitial melts are the mean of high SiO_2 GIC granitic compositions. In HC3, the felsic liquid is the mean of felsic segregations of the Upper Gabbros with non-zero MgO contents.

Table 2. Isotope data from the GIC and Hornitos plutons

Sample #	Map Unit	SiO_2 (wt. %)	Rb	Sr	$^{87}Rb/^{86}Sr$	$^{87}Sr/^{86}Sr$	Age (Saleeby et al. 1989)	$^{87}Sr/^{86}Sr$-initial
GP-GIC-1-2	Gabbro (felsic dike)	74.1	141	59	6.907	0.718879	151	0.70407
KP-GIC-G1	Gabbro	50.8	6	206	0.089	0.703442	151	0.70325
KP-GIC-AD1	Mingled zone (enclave)	60.2	56	208	0.775	0.705586	151	0.70392
KP-GIC-AH1	Mingled zone (granite host)	73.8	113	72	4.535	0.712286	151	0.70256
MD 16.2	Meladiorite	63.8	31	217	0.409	0.704451	151	0.70357
Smith 25	Granophyre	74.4	93	76	3.518	0.712188	151	0.70464
Smith 27B	Granophyre	74.4	113	44	7.387	0.719308	151	0.70347
KP-H-1	Hornitos	49.9	4	78	0.154	0.703892	151	0.70356
22	Hornitos	51.8	0	188	0.008	0.703836	150	0.70382
Smith 29-4	Low K2O Granophyre	65.8	2	200	0.024	0.705734	151	0.70568
Smith 29	Low-K2O Granite	64.5	11	224	0.145	0.706168	151	0.70586
G 13.5	Granophyre	66.2	41	98	1.221	0.705307	151	0.70269
KP-GIC-G1-2	Granophyre	74.4	2	136	0.033	0.706941	151	0.70687
J-2-8	Hypabyssal Mafic Porphyry	51.2	12	284	0.118	0.704558	160	0.70429
J-3-1	Bullion Mountain	55.0	1	339	0.005	0.704569	200	0.70455
J-7-1	Penon Blanco	61.4	26	342	0.222	0.705289	200	0.70466
J-8-3	159 Ma volcs. Greenstone	49.9	0	164	0.003	0.704512	160	0.70450
J-8-4	159 Ma volcs. Amphibolite	50.4	0	183	0.004	0.702936	160	0.70293
KP-GIC-R1	Rhyolite on top of GIC	69.2	34	432	0.227	0.708296	151	0.70781